Chemical Science

ROYAL SOCIETY OF CHEMISTRY

REVIEW

View Article Online
View Journal | View Issue

Check for updates

Cite this: *Chem. Sci.*, 2024, **15**, 9026

Photocatalytic NO_x removal and recovery: progress, challenges and future perspectives

Ting Xue,[a] Jing Li,[a] Lvcun Chen,[b] Kanglu Li,[b] Ying Hua,[a] Yan Yang *[cd] and Fan Dong *[a]

Received 21st March 2024
Accepted 18th May 2024

DOI: 10.1039/d4sc01891e

rsc.li/chemical-science

The excessive production of nitrogen oxides (NO_x) from energy production, agricultural activities, transportation, and other human activities remains a pressing issue in atmospheric environment management. NO_x serves both as a significant pollutant and a potential feedstock for energy carriers. Photocatalytic technology for NO_x removal and recovery has received widespread attention and has experienced rapid development in recent years owing to its environmental friendliness, mild reaction conditions, and high efficiency. This review systematically summarizes the recent advances in photocatalytic removal, encompassing NO_x oxidation removal (including single and synergistic removal and NO_3^- decomposition), NO_x reduction to N_2, and the emergent NO_x upcycling into green ammonia. Special focus is given to the molecular understanding of the interfacial nitrogen-associated reaction mechanisms and their regulation pathways. Finally, the status and the challenges of photocatalytic NO_x removal and recovery are critically discussed and future outlooks are proposed for their potential practical application.

1 Introduction

Nitrogen oxides (NO_x, consisting of 95% NO and NO_2) are pervasive air pollutants which are implicated in various environmental events (acid rain, photochemical smog, and global warming) and cause detrimental impacts on public health.[1–3] They serve as key precursors for the formation of emerging tropospheric ozone, $PM_{2.5}$ as well as secondary organic aerosol pollution.[2,4] Although there are NO_x from natural sources, anthropogenic activities, particularly fossil fuel combustion, account for a major contribution to the global NO_x emissions in the atmosphere.[5,6]

While NO_x is a pollutant, it can also be recognized as an energy feedstock. With a high reactivity, NO_x possesses the potential to be utilized for the synthesis of valuable N-containing chemicals. Ammonia (NH_3) is indeed an indispensable chemical for fertilizers,[7] dyes,[8] polymers,[9] explosives,[10] resins,[10] *etc.*, and can serve as a carbon-neutral energy carrier.[11] The industrial production of NH_3 synthesis currently heavily relies on the Haber–Bosch route, which requires harsh conditions (400–500 °C, 150–300 atm), resulting in more than 2% of global energy consumption.[12,13] This high energy consumption is also largely derived from fossil fuels.[14] Faced with global energy shortages, recovery of NO_x to NH_3 gives an alternative route for both environmental control and nitrogen resource utilization.

Photocatalytic technology powered by renewable solar energy has been reckoned as one of the most viable strategies that could convert NO_x into less harmful or useful products under mild conditions.[15–17] At present, conventional photocatalytic technologies, including NO_x oxidation, NO_x decomposition, and selective NO_x reduction, have been vigorously developed, spanning from material design to elucidation of the underlying mechanisms.[6,18–20] Meanwhile, the tendency of photocatalytic removal of NO_x has been gradually transformed from oxidation, purification, and then to resource utilization. Particularly, the photocatalytic NO_x reduction for ammonia synthesis has achieved milestone progress in recent years.

The review aims to summarize recent advancements in photocatalytic NO_x removal and recovery. The cutting-edge developments in photocatalytic removal in terms of NO_x oxidation, NO_x reduction to nitrogen, and NO_x upcycling to ammonia are comprehensively reviewed. We also highlighted the one-step ($NO \rightarrow NH_3$) and two-step ($NO \rightarrow NO_3^- \rightarrow NH_3$) methods as new ideas for simultaneous NO_x removal and resource utilization. Finally, we discuss the current challenges and provide some perspectives on future directions for NO_x removal and recovery. The illustration of this review on NO_x removal and recovery is shown in Scheme 1. We hope that this

---

[a] *Research Center for Carbon-Neutral Environmental & Energy Technology, Institute of Fundamental and Frontier Sciences, University of Electronic Science and Technology of China, Chengdu 611731, China. E-mail: dongfan@uestc.edu.cn*

[b] *School of Environmental Science and Engineering, Southwest Jiaotong University, Chengdu 611756, China*

[c] *School of Chemical Engineering and Light Industry, Guangdong University of Technology, Guangzhou 510006, China. E-mail: yangyan1209@gdut.edu.cn*

[d] *Synergy Innovation Institute of GDUT, Shantou, 515041 Guangdong, China*

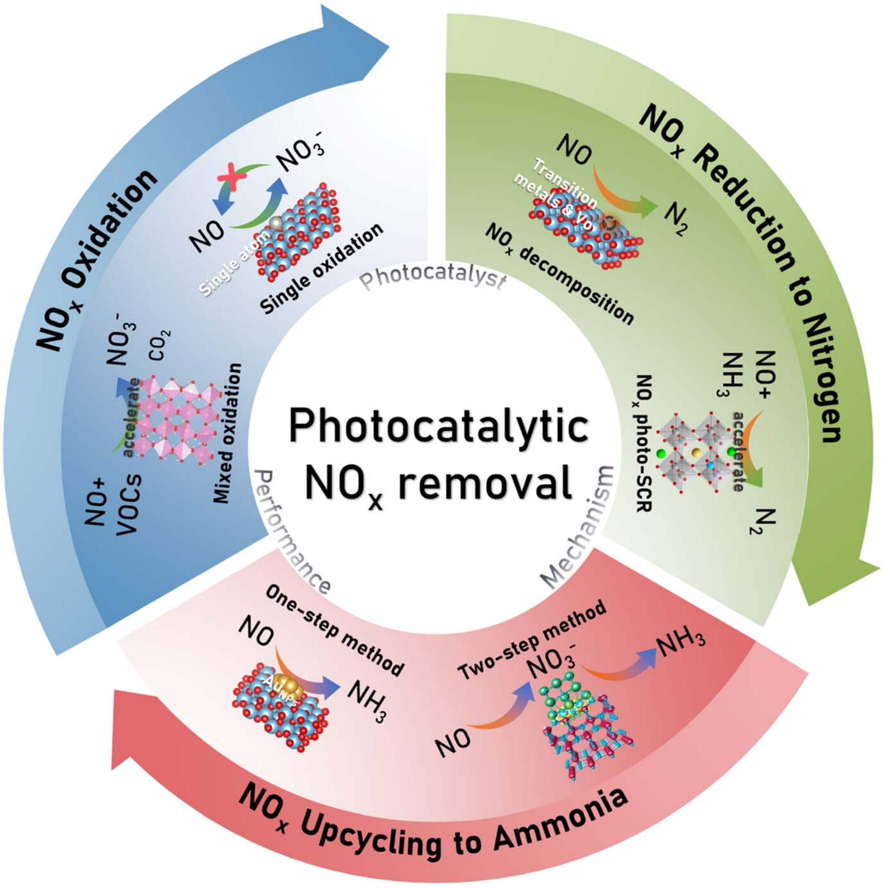

Scheme 1 The NO_x removal and recovery by different photocatalytic approaches.

review will inspire significant research and essential advancements in the field of photocatalytic NO_x removal.

2 NO_x oxidation

2.1 Single NO_x oxidation

2.1.1 NO_x oxidation mechanisms. Photocatalytic oxidation removal is mainly applied to low-concentration pollutant purification. During the photocatalytic reaction process, electron–hole pairs are generated in the catalyst under light irradiation, initiating the oxidation reactions. These pairs migrate to the surface of the photocatalysts and react with adsorbed H_2O and O_2 molecules, leading to the generation of reactive oxygen species (ROS) such as $^{\bullet}OH$, $^{\bullet}O_2^-$, and $^1O_2$. These ROS then participate in a series of oxidation reactions with NO, ultimately forming the final product NO_3^-. Detailed reaction pathways and intermediates involved in this photocatalytic NO oxidation process can be described using specific equations, which are supported by relevant ref. 21 and 22:

$$\text{Photocatalysts} + h\nu \rightarrow h^+ + e^- \tag{1}$$

$$H_2O + h^+ \rightarrow {}^{\bullet}OH + H^+ \tag{2}$$

$$NO + {}^{\bullet}OH \rightarrow HNO_2 \tag{3}$$

$$HNO_2 + {}^{\bullet}OH \rightarrow NO_2 + H_2O \tag{4}$$

$$NO_2 + {}^{\bullet}OH \rightarrow NO_3^- + H^+ \tag{5}$$

$$O_2 + e^- \rightarrow {}^{\bullet}O_2^- \tag{6}$$

$$NO + {}^{\bullet}O_2^- \rightarrow NO_3^- \tag{7}$$

$$O_2^- + h^+ \rightarrow {}^1O_2 \tag{8}$$

$$NO + {}^1O_2 \rightarrow NO_3^- \tag{9}$$

2.1.2 Materials for NO_x oxidation. There are three main factors affecting the catalytic performance of photocatalytic oxidation: light absorption, charge carrier separation and transfer, and active site construction.[23] Based on these factors, various modification methods were conducted on TiO_2-based materials,[24–27] Bi-based materials,[28–30] $g\text{-}C_3N_4$-based materials,[31,32] and perovskite-type materials.[33] Modification methods include but are not limited to metal/non-metal doping, defects, heterojunctions, and sensitization.[34]

Single-atom catalysts have attracted much attention in the field of materials due to their unique activity and effective utilization of active atoms. Several studies have confirmed that single atoms can improve the performance of photocatalysts for

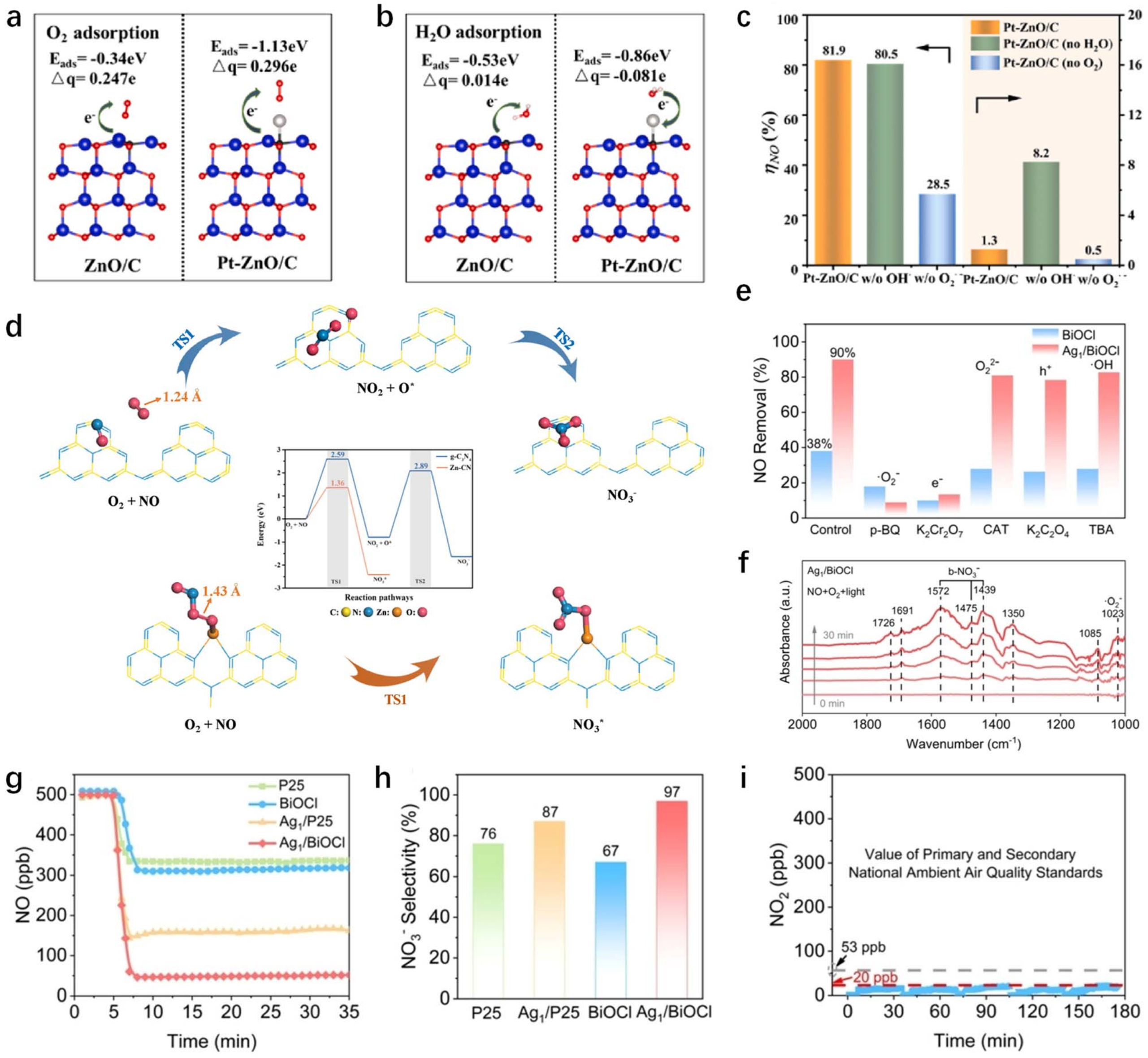

Fig. 1 DFT calculation of (a) O_2 adsorption and (b) H_2O adsorption on ZnO/C and Pt–ZnO/C surfaces. (c) The NO conversion rate and selectivity of NO_2 formation over the Pt–ZnO/C catalyst in the presence and absence of moisture and O_2.[36] (d) NO oxidation process over g-C_3N_4 and Zn–CN.[37] (e) Photocatalytic NO removal over Ag_1/BiOCl using different scavengers. (f) DRIFTS spectra of Ag_1/BiOCl for NO oxidation. (g) NO oxidation of P25, BiOCl, Ag_1/P25 and Ag_1/BiOCl. (h) NO_3^- selectivity of Ag_1/P25 and Ag_1/BiOCl under visible light irradiation. (i) The amount of NO_2 generation.[39]

NO_x removal and provide a convenient way to regulate the generation of ROS for effective pollutant elimination. Liu *et al.*[35] achieved the stabilization of Pt on carbon-defective g-C_3N_4 by leveraging its affinity with nitrogen atoms resulting from carbon vacancies. The resulting Pd-C_v-CN catalyst enhances charge transfer efficiency, generating sufficient photoelectrons for the formation of $^{\bullet}OH$ and $^{\bullet}O_2^-$ species. This, in turn, facilitates the removal of NO and enhances the selectivity towards NO_3^-. Hu *et al.*[36] discovered that single Pt atom bridged within a metal–organic framework (MOF)-derived ZnO/C *via* carbon atoms (Pt–ZnO/C) exhibits enhanced adsorption energy and charge transfer characteristics for O_2 and H_2O (Fig. 1a and b). In contrast to $^{\bullet}OH$, $^{\bullet}O_2^-$ plays a pivotal role in the conversion of NO_x to NO_3^- on a single atom site at the catalytic surface (Fig. 1c). Zhang *et al.*[37] incorporated Zn atoms into the interlayer of g-C_3N_4, forming the ZnN_3 structure by linking zinc with three nitrogen atoms. The presence of a single zinc atom facilitated the formation of a Zn–O_2–NO structure upon adsorption of O_2 and NO, thereby promoting the dissociation of O_2 and the direct conversion of NO to nitrate (Fig. 1d). Simultaneously, the formation of the toxic byproduct NO_2 was inhibited. A similar result enhancement was observed upon doping TiO_2 hollow microspheres (TiO_2-HMSs) with single atomic Fe.[38] Particularly noteworthy is the effect of silver atoms loaded onto BiOCl (001) facet-exposed nanosheets, which constructed triangular Cl–Ag_1–Cl sites on Cl-terminated BiOCl. These sites selectively activated molecular oxygen to $^{\bullet}O_2^-$ and enhanced nitrate adsorption by altering the coordination mode of nitrate on the catalyst, thereby preventing nitrate decomposition (Fig. 1e and f).[39] The NO_x removal efficiency of Ag_1/BiOCl reached up to 90%, with 97% selectivity for NO_3^- and minimal emission of NO_2 (Fig. 1g–i).

In summary, the introduction of single atoms can significantly enhance the adsorption of O_2 and H_2O molecules and the generation of $^{\bullet}O_2^-$ and $^{\bullet}OH$, thereby improving both the performance and nitrate selectivity of the photocatalyst. This provides a facile pathway to manipulate the ROS generation for efficient and selective pollutant removal.

2.1.3 Machine learning as an analysis tool for NO_x oxidation. It is well-known that the performance of NO_x removal not only depends on catalyst properties but also closely relies on preparation methods and reaction conditions. Although catalyst design and optimization of experimental conditions have been fully explored, the dominant factors affecting the NO_x removal rate remain unclear. Machine learning (ML) has achieved remarkable progress over the past few decades and has become the most potent tool in the field of data mining and analytics.[40,41] ML methods leverage algorithms to extract insights from vast, intricate, and multidimensional datasets, enabling rapid and precise predictions. Recently, progress has been made in employing ML methods in the photocatalytic NO_x oxidation process. Li *et al.*[42] achieved success in predicting the NO removal rate in the photocatalytic purification of g-C_3N_4 catalysts using ML methods like gradient boosting decision trees, eXtreme gradient boosting, and random forests. Their findings indicate that catalyst characteristics, reaction process, and preparation conditions are the primary empirical categories influencing the NO removal rate. They have also unveiled the intricate relationships between the photocatalytic NO removal rate and various influencing factors. This approach, to some extent, mitigates the downsides of traditional experimental work, including high costs, lengthy timelines, and demanding labor.

2.1.4 NO_3^- decomposition on the photocatalyst. The formation of nitrate is a key process of NO_x oxidation, as nitrate has been considered a permanent sink of NO_x.[43] However, it undergoes photolysis processes under light irradiation (also called detoxification), especially on the surface of the photocatalyst, which in turn serves as a source of atmospheric nitrogenated compounds.[44–49] TiO_2, the predominant photocatalyst,[50,51] has been shown to promote nitrate photolysis processes through photochemical interaction.[44] Therefore, exploring the decomposition mechanism of nitrate on the surface of photocatalysts assumes pivotal significance for stabilizing nitrate on the catalyst surface. The enhanced photolysis of nitrate by TiO_2 under UV irradiation can be explained using the following reactions[52–54] (eqn (10)–(19)):

$$TiO_2 + h\nu \rightarrow h^+ + e^- \tag{10}$$

$$NO_3^- + h^+ \rightarrow NO_3^{\bullet} \tag{11}$$

$$NO_3^{\bullet} + h\nu \rightarrow NO + O_2 \tag{12}$$

$$NO_3^{\bullet} + h\nu \rightarrow NO_2 + O\bullet \tag{13}$$

$$NO_2 + h\nu \rightarrow NO + O(^3P) \tag{14}$$

$$NO_2 + e^- \rightarrow NO_2^- \tag{15}$$

$$NO_2 + 2e^- + 2H^+ \rightarrow NO + H_2O \tag{16}$$

$$2NO + 2e^- + 2H^+ \rightarrow N_2O + H_2O \tag{17}$$

$$NO_2^- + H_2O \rightarrow HONO + HO^{\bullet} \tag{18}$$

$$HONO + h\nu \rightarrow NO + HO^{\bullet} \tag{19}$$

There are two main factors affecting the nitrate decomposition mechanism on the TiO_2, which are co-adsorbed cations and the coexisting atmosphere. It is suggested that the cations on TiO_2 could inhibit the decomposition of nitrates. The presence of cations enhanced the adsorption of NO_3^- by forming ion pairs with NO_3^- and prevented NO_3^- from binding with light-induced h^+ to generate $^{\bullet}NO_3$.[55,56] The decomposition of nitrates is facilitated by co-existing pollutants in the surrounding environment such as SO_2 and volatile organic compounds (VOCs). SO_2 preferentially reacts with $^{\bullet}NO_3$ radicals rather than photoelectrons, resulting in a significant improvement in nitrate decomposition.[57,58] Similar to SO_2, formaldehyde (HCHO) participated in the transformation of NO_3 to HNO_3 through hydrogen abstraction to promote nitrate decomposition. HCHO converts NO_3^- on particle surfaces into HNO_3 by reacting with $^{\bullet}NO_3$, and then HNO_3 photolyzes at a faster rate.[55] Interestingly, NO produced from nitrate decomposition may be re-adsorbed on the surface of TiO_2 to promote nitrate decomposition.[59] The N–O bond of NO_3^- could be activated by NO molecules. Subsequently, photogenerated electrons, captured by NO, facilitate the transformation of NO_3^- under light irradiation through the $NO_3^- + NO^- \rightarrow 2NO_2^-$ pathway.[59] It is proposed that addressing the photochemical transformation of surface NO_3^- may entail suppressing the formation of NO^- during the photocatalytic NO oxidation process.

Although the well-known photochemical activity of nitrate decomposition is excited around 300 nm,[60] it has been verified that nitrate decomposition could be induced by visible light ($\lambda >$ 380 nm) on TiO_2. Wang *et al.*[47] investigated the decomposition of surface NO_3^- on nmTiO_2 under visible light exposure. By regulating the reaction atmosphere (dry argon, wet argon, and wet air), distinct production of NO and NO_2 is observed (Fig. 2a–c). Through meticulous control of *in situ* DRIFTS experiments, they uncovered different decomposition pathways stemming from different surface coordination modes of the NO_3^- (Fig. 2d and e). Nitrates generated on photocatalysts exhibit two coordination modes: monodentate nitrate (m-NO_3^-) and bidentate nitrate (b-NO_3^-). The m-NO_3^- decomposition initiated by photo-induced electrons primarily leads to the production of NO and NO_2. It is indicated that H_2O and O_2 have a remarkable

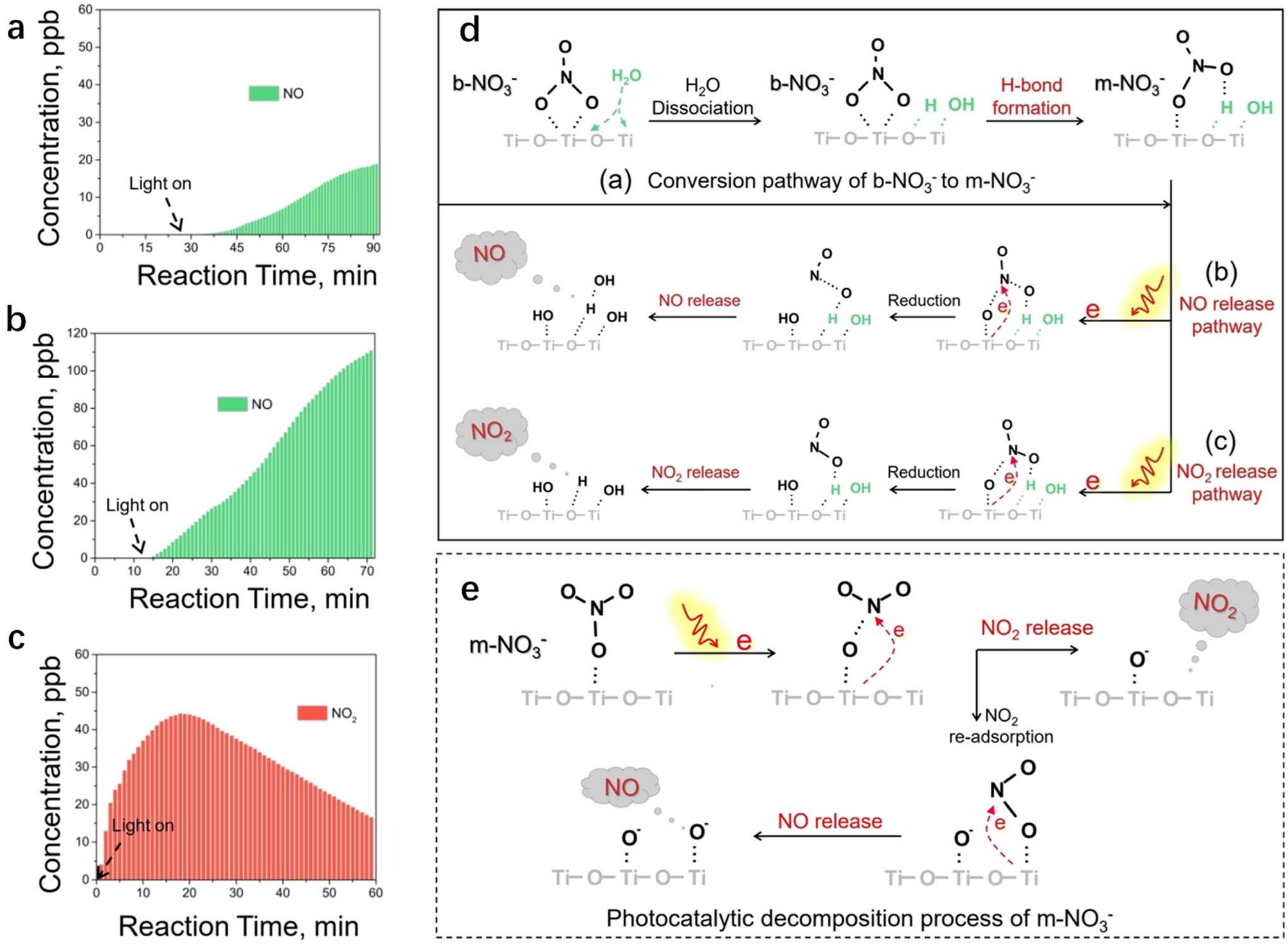

Fig. 2 Generation of gas-phase products in (a) dry argon atmosphere, (b) humidity argon atmosphere, and (c) humidity air atmosphere under visible light irradiation. (d) Proposed decomposition mechanism of b-NO_3^- triggered by visible light photocatalysis: (a) conversion pathway of b-NO_3^- to m-NO_3^- under visible light irradiation. (b) Photocatalytic decomposition pathway of produced m-NO_3^- to NO. (c) Photocatalytic decomposition pathway of produced m-NO_3^- to NO_2. (e) Proposed decomposition mechanism of m-NO_3^-.[47]

influence on the decomposition products of NO_3^-. The introduction of H_2O molecules results in dissociation on nmTiO_2, forming surface hydroxyl groups, which then facilitate the conversion of b-NO_3^- to m-NO_3^- through hydrogen bonding interactions.[47] Subsequently, visible-light-driven photocatalytic decomposition led to an enhancement in the concentration of NO_x. Although O_2 can promote nitrate regeneration through the oxidation process, the effect of H_2O on NO_3^- decomposition could not be restrained in the presence of O_2.

To sum up, the decomposition of nitrate on the surface of active particulate matter TiO_2 under various conditions has been confirmed. Therefore, when exploring the mechanism of oxidative NO_x removal, it is essential to consider the nitrate decomposition process. This perspective offers valuable insights for a more comprehensive understanding of the photocatalytic reaction.

2.2 Synergistic NO_x oxidation

In the real scenario, NO_x is typically present alongside other air pollutants. The interaction or combination of NO_x with other pollutants, such as volatile organic compounds (VOCs) and sulfur dioxide (SO_2), can lead to the formation of more severe secondary pollutants, especially under sunlight irradiation.[61–65] In addition to designing effective photocatalysts, it is crucial to address the complexities arising from these multiple pollutants when implementing photocatalytic NO oxidation technology in real reactors at pilot or larger scales.[66]

2.2.1 Synergistic effect between NO_x and VOCs. It has been revealed that there is a certain synergistic effect between NO_x and VOCs on the specific photocatalysts to inhibit the generation of by-products. Xue *et al.*[67] proposed an enhanced photocatalytic NO removal through the addition of acetaldehyde to $Sr_2Sb_2O_7$ to prevent secondary peroxyacetyl nitrate (PAN) formation. The intermediates NO_2^- from NO and $^{\bullet}CH_3$ from acetaldehyde tend to bond and further oxidize to CH_3ONO_2, thus promoting NO removal. Density functional theory (DFT) calculations show that the Gibbs free energy required for the conversion of NO to NO_3^- in the mixed degradation process is lower compared to that in the individual removal pathways, thereby favoring the deep oxidation to NO_3^-. Li *et al.*[68]

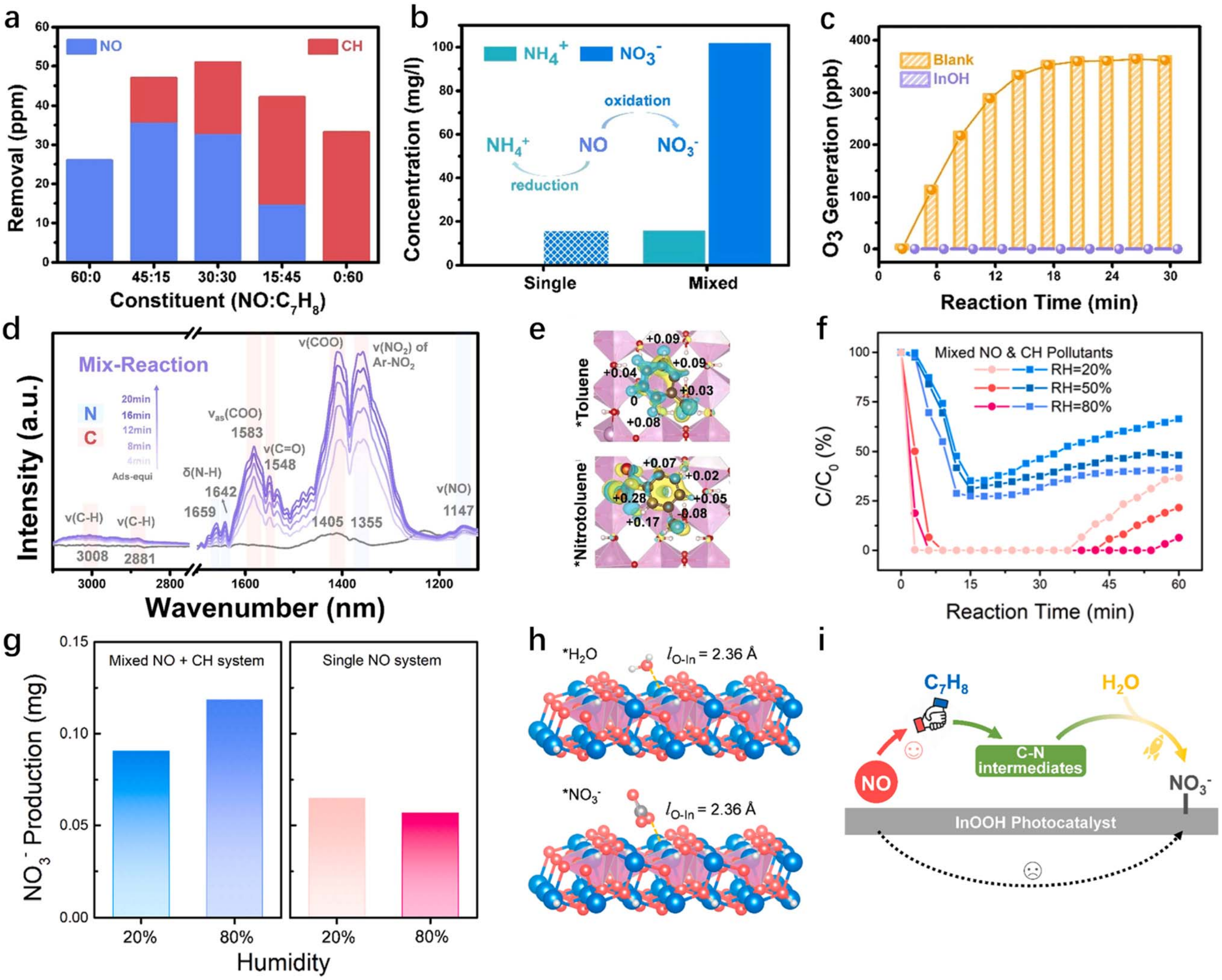

Fig. 3 (a) The removal of NO and C_7H_8 at different mixing ratios. (b) The nitrogen-containing products identified by IC. (c) The generation of O_3 without and with the photocatalyst under light irradiation. (d) *In situ* DRIFTS spectra for the photocatalytic reaction of NO and C_7H_8.[68] (e) Charge distribution of C_7H_8 and $C_7H_7NO_2$ on the $In(OH)_3$ photocatalyst; blue and yellow clouds represent charge depletion and accumulation, and the isosurface level is set to 0.0007 eV Å^{-3}. (f) Conversion of mixed pollutants at different relative humidities. [NO] = [C_7H_8] = 30 ppm. (g) NO_3^- production in mixed and single systems at different relative humidities. (h) Simulation of reactant and product binding on the catalyst. (i) Illustration of the synergistic interaction between NO and C_7H_8 and the promoting effect of H_2O.[69]

investigated the simultaneous degradation of NO and C_7H_8 (toluene) mixed pollutants. On the $In(OH)_3$ photocatalyst, NO and toluene exhibit coupling reaction effects and give rise to a new NO conversion pathway, leading to NO deep oxidation to NO_3^- (Fig. 3a and b). The key intermediate C_7H_7NOH is favorable for the NO oxidation to NO_2 to inhibit O_3 formation (Fig. 3c and d). Then NO_2 was inclined to bond with toluene to form $C_7H_6NO_2$. The incorporation of the nitro group alters the charge distribution within the benzene ring, disrupting the typical distribution of electrons within the π–π stacked structure (Fig. 3e). The rearrangement of electrons opens the benzene ring more readily than toluene, allowing further NO_3^- formation. This synergistic effect of NO and toluene also occurs in InOOH. The increase in humidity could suppress catalyst deactivation and improve the conversion of mixed pollutants, as shown in Fig. 3f.[69] The yield of nitrate is also consistent with the conversion efficiency (Fig. 3g). This finding indicates that the extensive occupation of the catalyst surface by nitrate serves as a deactivation factor in mixed pollutant reactions.[69] Under high humidity conditions, H_2O and NO_3^- indicate similar adsorption configurations on InOOH, but H_2O generates more free radicals to directly enhance the conversion of C–N intermediates, thus promoting the conversion of NO to NO_3^- (Fig. 3h and i).[69] It was also proposed that NO could prevent the deactivation of the photocatalyst due to the incomplete oxidation product NO_2 in the process of o-xylene degradation.[70] NO_2 ensures the generation of a sufficient amount of TiO_2 ($^{\bullet}$OL) radicals, allowing for the complete mineralization of o-xylene and inhibiting the deactivation of TiO_2.[70]

2.2.2 **Inhibition effect between NO_x and SO_2.** In contrast to VOCs, research indicates that SO_2 tends to hinder the removal of NO_x. According to the studies of Ao *et al.*,[71] the presence of

SO_2 resulted in an 8% decrease in NO conversion and a 10% increase in NO_2 generation. The formation of sulfate ions on the catalyst surface obstructed the adsorption sites of TiO_2 for converting NO_2 to HNO_3, consequently increasing the exit concentration of NO_2. Chen *et al.*[66] further validated this deactivation mechanism through DFT calculations. The result showed that surface hydroxyls on the (101) facet of TiO_2 create unsaturated coordination of adjacent Ti or O atoms, promoting the adsorption of NO and SO_2. However, there is a competitive adsorption between NO and SO_2, as evidenced by the decreasing adsorption energy and charge density. In the oxidation process, SO_2 significantly competes with NO for reaction with $^{\bullet}O_2^-$. More valence electrons are involved in the oxidation of SO_2, resulting in higher binding energy between *O–SOOO* than *O–NOO*.

3 NO_x reduction to nitrogen

Contemporary research in photocatalytic NO abatement predominantly centers on oxidizing NO to NO_3^-. Nevertheless, concerns arise from the production of the more toxic by-product, NO_2, catalyst deactivation resulting from the obstruction of reaction sites by nitrate products, and the denitrification of NO_3^-. These challenges impede the practical application of photocatalysts. An alternative approach for NO_x removal involves the reduction of NO to N_2 without causing deactivation or secondary pollution. This can be achieved through two approaches: direct reduction of NO to N_2 and O_2 under oxygen-free conditions (NO_x decomposition), and selective reduction of NO to N_2 in a reducing atmosphere (NO_x photo-selective reduction).

3.1 NO_x decomposition

The decomposition of NO into harmless N_2 and O_2 represents one of the most desirable pathways of NO removal, as it eliminates the need for additional reductants. Transition metal oxides have emerged as typical photocatalysts for NO_x decomposition.[72–82] Utilizing zeolite supports allows for the production of highly dispersed powders, enhancing the performance of NO decomposition.[83] Previous studies have demonstrated the significant contribution of transition metal ions to the photocatalytic NO decomposition. As shown in eqn (20), highly dispersed and isolated transition metal oxides form the charge-transfer excited states under irradiation, which involve electron transfer from $O_{(l)}^{2-}$ to $M_{(l)}^{n+}$:

$$\left[M^{n+}-O^{2-}\right]_{(l)}+h\nu\rightarrow\left[M^{(n-1)+}-O^{-}\right]_{(l)}^{*}\quad M=\text{Ti, V, Cr, Mo}\ldots \tag{20}$$

The selectivity of N_2 increases as the coordination number of the M–O bond decreases, which triggers the photocatalytic decomposition of NO.[83] It was shown that the Ti-oxide/Y-zeolite catalysts with tetrahedral coordination exhibit higher reactivity and selectivity for N_2 generation and lower selectivity for N_2O formation than those with octahedral coordination.[83] The performance of the photoreduction reaction could also be improved by oxygen vacancies and doping the catalyst with transition metals.[81,82] van de Krol *et al.*[82] doped TiO_2 nanoparticles with Fe^{3+}, which changed the photocatalytic NO removal route from oxidation to reduction (Fig. 4a). The Fe^{3+} substituted Ti^{4+} in the lattice, and the negative charge of this acceptor-type dopant contributed to the stabilization of positivity-charged oxygen vacancies. The oxygen vacancies could act as active sites to capture the molecular O of the NO molecule and provide light-induced electrons (Fig. 4b). Besides, Ag^0 and Ag^+ coexist on the TiO_2 surface, which both play different roles in the enhancement of N_2 selectivity: the Ag^0 nanoparticles enhance the light absorption of the material, while Ag^+ can decompose the attachment product N_2O into N_2.[81] A recent study shows that layered structured perovskite $SrBi_2Nb_2O_9$ with ultrathin nanostructure and oxygen vacancies (SBNO-UT) is capable of decomposing NO into N_2 and O_2 at the close-to-stoichiometric ratio (Fig. 4c).[84] As can be seen from Fig. 4d, N_2O intermediates were formed by NO reduction during the photocatalytic process. The *in situ* formed N_2O bounds to the defective surface, ensuring further reduction (Fig. 4e). Finally, the breakage of the N=O bond completes the reduction of NO to N_2.

3.2 NO_x photo-selective reduction

The method of selectively converting NO to N_2 by introducing reducing agents such as NH_3, CO, H_2, and hydrocarbons into the system is known as selective catalytic reduction (SCR). Despite extensive study,[85,86] the technology typically operates at high temperatures (300–400 °C),[87,88] leading to relatively high energy consumption and potentially excessive CO_2 emissions. In addressing these challenges, photo-assisted SCR (photo-SCR) of NO_x with NH_3 using photocatalysts under light irradiation and low-temperature conditions has been developed as an alternative for NO_x reduction.

NH_3 serves as a common reductant for NO_x removal by photo-SCR, with TiO_2 being the most extensively utilized catalyst in this system. The reaction mechanism of NO photo-SCR with NH_3 on TiO_2 is depicted in Fig. 5a.[89] There are numerous TiO_2-based materials for photo-SCR, *e.g.*, TiO_2/SiO_2,[90] TiO_2 nanotube arrays,[91] Bi_2WO_6/TiO_2 Z-scheme heterojunctions,[92] g-C_3N_4/TiO_2 (ref. 93) and Pd-loaded TiO_2,[94] and Si/TiO_2.[95] Tanaka *et al.*[96] reported achieving the photocatalytic selective reduction of NO with NH_3 using TiO_2 under xenon lamp illumination at conversion temperatures as low as 50 °C. They also investigated the activity of TiO_2 surfaces loaded with 1 wt% of various transition metal oxides.[97] Their findings revealed that Nb, Mo, and W oxides promoted the photo-SCR activity of TiO_2, with WO_3/TiO_2 exhibiting the highest activity (Fig. 5b). The number of acidic sites on TiO_2 as active sites for the photo-SCR reaction determines the reactivity of the photocatalyst.[98] Modification of TiO_2 with WO_3 resulted in increased polarizability, enhancing the surface acidity and thus facilitating the reduction of NO.[99,100] Subsequent studies concluded that agglutination occurs with increasing WO_3 addition, with isolated W species enhancing the chemical reduction activity of NO, while agglutinated W species remain inactive.[101]

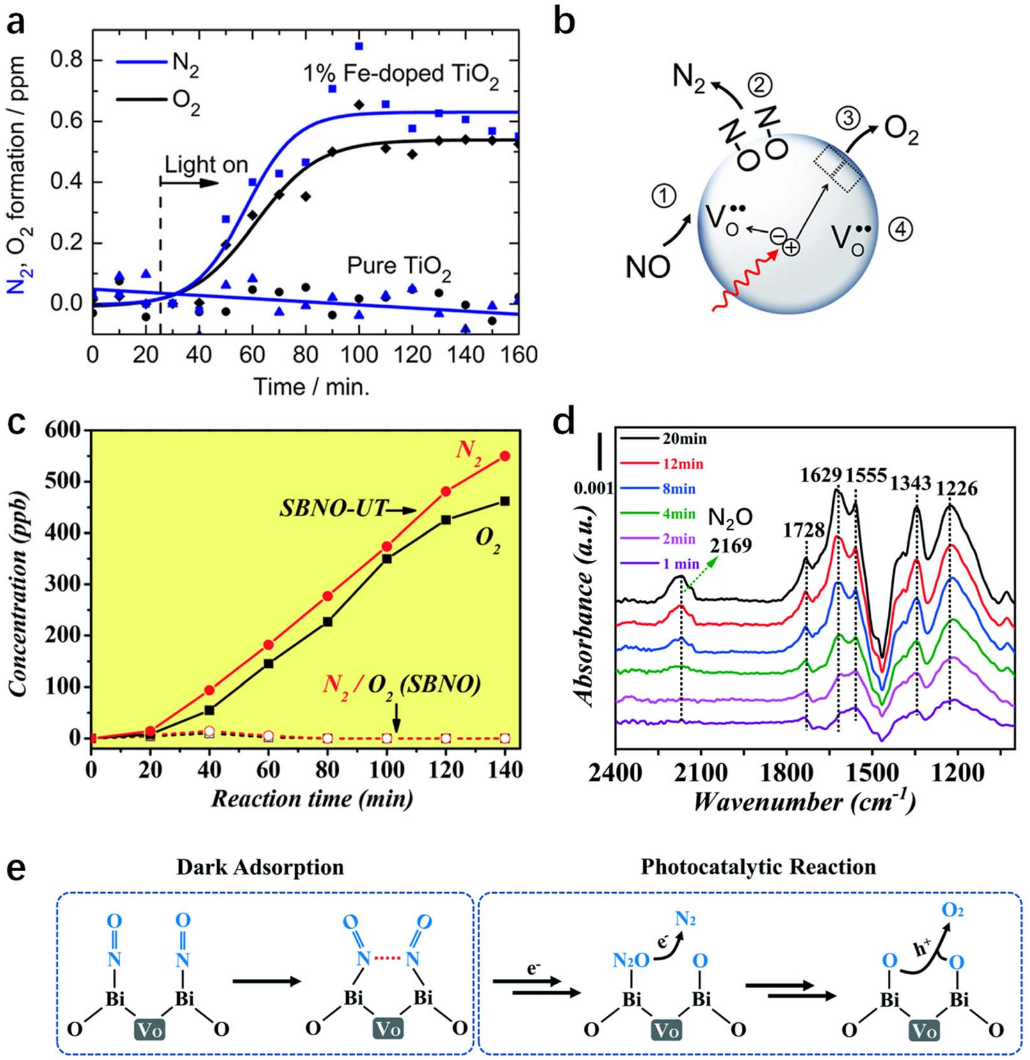

Fig. 4 (a) Photocatalytic conversion of NO to N_2 and O_2 over 1% Fe-doped TiO_2. The sample was irradiated with UV light, and the target pollutant was 100 ppm NO in He. (b) Possible elementary reaction routes of NO on Fe-doped TiO_2.[82] (c) Formation of photocatalytic NO decomposition products on SBNO and SBNO-UT, respectively, in a sealed system with 13.5 ppm NO. (d) *In situ* FTIR spectra of SBNO-UT during the photocatalytic NO abatement (0–20 min). The background was collected after the equilibrium of NO adsorption was reached but before illumination. (e) Possible mechanism of the photocatalytic NO decomposition on SBNO-UT.[84]

Perovskite (ABO_3) structured materials with flexible structures have recently garnered scientific interest for their application in photo-SCR. Researchers have synthesized Ce–Fe–Mn doped $CaTiO_3$ perovskite from titanium-containing solid waste using the molten salt method.[103] Fig. 5c–e illustrate that $CaTiO_3$ showed no photocatalytic activity for NO removal at temperatures ranging from 100 to 300 °C. However, (Ca, Ce) (Ti, Mn, Fe) O_3 demonstrated almost 100% NO conversion under light irradiation at 135 °C (GHSV = 72 000 h^{-1}). Both Mn and Fe are incorporated into the B-site of $CaTiO_3$, while Ce occupies the A-site. Mn doping enhances material light absorption and the capacity to capture NO. After Fe doping, the oxidation center for NO-to-NO_3^- shifts from the five-coordinated Mn_{5c} site to the Fe_{5c} site, significantly altering the reaction pathway of conventional SCR. Furthermore, Pr doping of $LaCoO_3$ supported on a natural palygorskite (Pal) surface eliminates over 95% of NO_x within the low-temperature range of 150–250 °C.[104] Appropriate Mn doping into $LaFeO_3$ to form $LaFe_{1-x}Mn_xO_3$/attapulgite (ATP) nanocomposites extends its visible light absorption range, resulting in increased NO conversion, reaching a maximum of 85%, with N_2 selectivity close to 100%.[87] Ni-doped $LaFeO_3$ nanocomposites exhibit a higher NO_x conversion rate of 92%.[105] Moreover, nitrogen-doped carbon quantum dot modified $PrFeO_3$/Pal, with abundant acid sites, demonstrate 93% NO removal and 100% N_2 selectivity under visible light illumination, showing considerable tolerance to SO_2 and H_2O.[106]

4 NO_x upcycling to ammonia

The upcycling of NO_x to ammonia presents an environmentally friendly opportunity for both NO_x pollutant elimination and

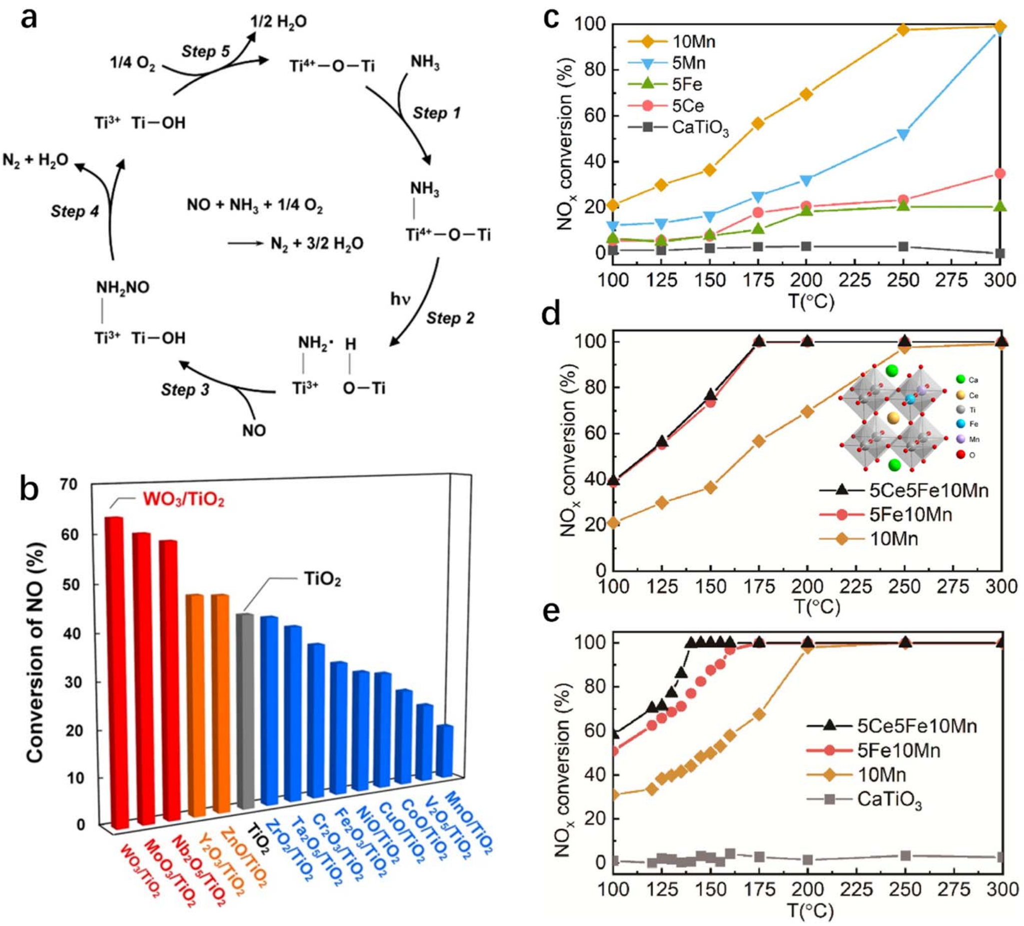

Fig. 5 (a) Proposed reaction mechanism of the photo-SCR over a TiO_2 photocatalyst under UV-light irradiation.[89] (b) Conversion of NO in the photo-SCR over various metal oxide-promoted TiO_2 photocatalysts.[102] (c–e) NH_3-SCR activity of single- and multi-element doped $CaTiO_3$.[103]

sustainable ammonia production. While electrocatalytic synthesis of ammonia has garnered considerable attention, photocatalytic reduction of NO to ammonia remains in its nascent stage. Nevertheless, recent years have seen significant advancements in photocatalytic ammonia synthesis. The authors outline two potential approaches for NO_x resource utilization *via* photocatalysis. One method involves the use of a chelating agent with the dissolution of NO in water, followed by a one-step reduction to ammonia *via* photocatalysis (one-step method). Another approach entails oxidizing NO to the highly water-soluble NO_3^- initially, followed by its reduction to ammonia through an eight-electron reduction process (two-step method).

4.1 One-step method (NO → NH_3)

The direct one-step synthesis of NH_3 from NO is an ideal strategy for transforming waste into valuable resources. While research efforts in NO_x reduction reactions (NO_xRR) have predominantly focused on enhancing NH_3 synthesis rates, achieving high NO_x conversion efficiency remains a crucial yet less explored objective.[107,108] Typically, NO_xRR experiments necessitate efficiency tests with high concentrations (>10 000 ppm) of NO to ensure an adequate feedstock for enhancing ammonia production.[109] However, limited NO conversion persists as a key challenge for the sustainability of the NO-to-NH_3 reduction pathway.

The ultra-low solubility of NO in water (1.94 mmol L^{-1}) is one of the primary reasons for limited NO conversion.[110] To address this challenge, a novel one-step NO_x photoreduction pathway, referred to as the on-site coupling system, has been recently developed. This system enables NO direct upcycling under ambient conditions (Fig. 6a).[111] Specifically, the solution was supplemented with Fe(II)EDTA as a NO chemical absorbent, generating Fe(II)EDTA-NO chelates, while formaldehyde (HCHO) served as an antioxidant to prevent the Fe(III) formation from Fe(II) oxidation. This simultaneous chemical absorption and photocatalytic reduction system enabled continuous NO adsorption, NO reduction, and Fe(II)EDTA regeneration on-site.[111] TiO_2 decorated with 11.6 mg L^{-1} Au nanoparticles could provide ample active sites to facilitate charge separation, thereby enhancing NH_4^+ generation. Using this on-site coupling system, the performance of Au_{NPs}–TiO_2 is shown in Fig. 6b and c, demonstrating exceptional NO conversion efficiency (89.0%), ammonia production selectivity (95.6%), and ammonia recovery efficiency (>90%). Virtually no other side products are detected. Subsequently, the generated ammonia was recovered *via*

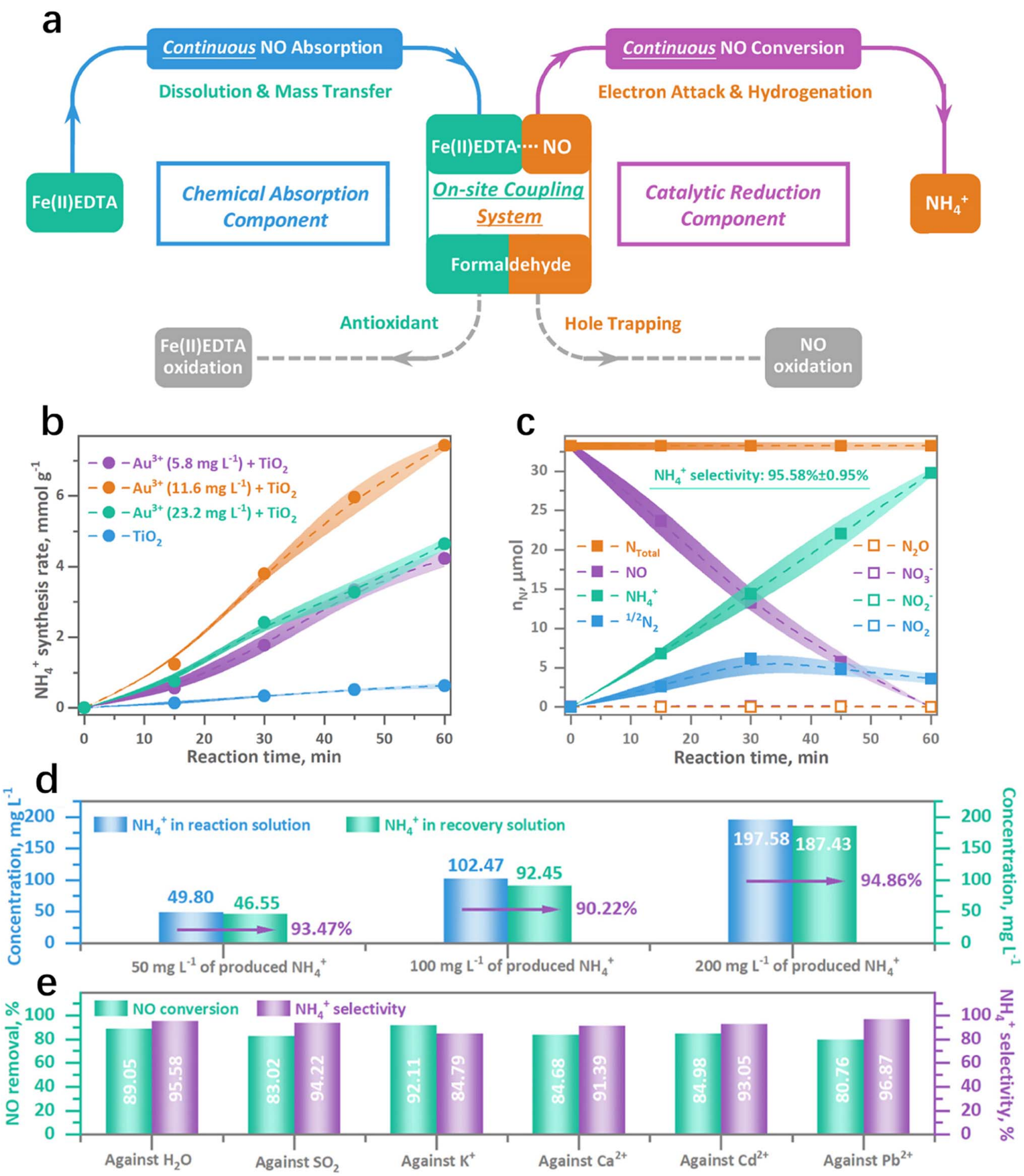

Fig. 6 (a) Illustration of the on-site coupling system of continuous chemical absorption and catalytic reduction. (b) NH_4^+ synthesis rate between the pristine and Au-decorated TiO_2. (c) Selectivity test. (d) Ammonia recovery evaluation after the continuous absorption and photoreduction of NO. (e) Poisoning resistance against vapor, SO_2, and metals.[111]

a simple ion exchange method, with recovery rates still exceeding 90% within 50–200 mg L^{-1} ammonia production (Fig. 6d). Moreover, the NO conversion efficiency and the NH_4^+ selectivity remained unaffected even in the presence of resistance factors such as H_2O, SO_2, and metal ions (K^+, Ca^{2+}, Cd^{2+}, and Pb^{2+}) (Fig. 6e). These high recovery efficiencies and anti-poisoning capacities underscore the environmental practicality of NO_x removal in flue gas. The on-site coupling strategy achieves significant efficiency milestones for sustainable NO

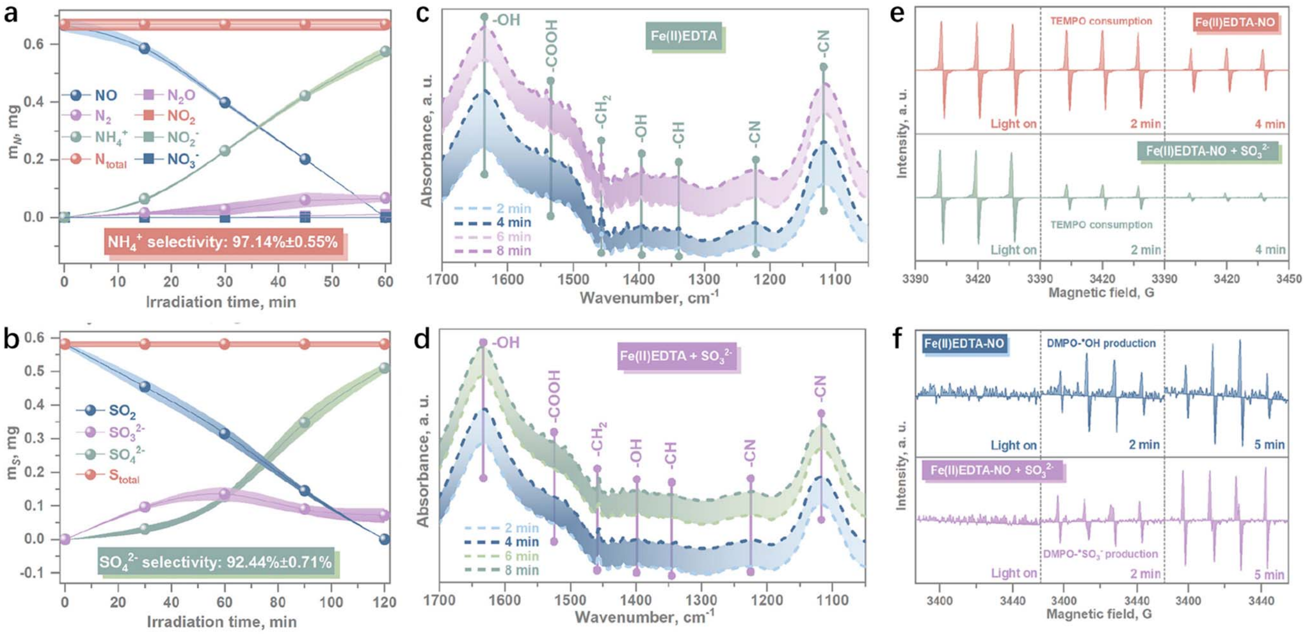

Fig. 7 The continuous selectivity evaluation for (a) NO-to-NH_3 reduction and (b) SO_2-to-SO_4^{2-} oxidation. *In situ* ATR-FTIR spectra for the recording of Fe(II)EDTA characterization signals (c) without and (d) in the presence of SO_3^{2-} provision. (e) *In situ* EPR measurements for the consumption of TEMPO in the photocatalytic reduction process of NO without (up) and with (down) SO_3^{2-} provision, respectively, (f) *In situ* EPR measurements for the production of DMPO-$^\bullet$OH by H_2O oxidation (up) and DMPO-$^\bullet SO_3^-$ by SO_3^{2-} oxidation (down), respectively.[114]

removal and also offers insights into NO upcycling for the future of carbon neutrality.

The simultaneous presence of NO and SO_2 in flue gas poses significant challenges for their concurrent removal and recovery.[112,113] Since SO_2 is easily dissolved and oxidized, it can serve as a potential reductant in the NO photoreduction reaction. Furthermore, the on-site coupled system demonstrated the synergistic removal and recycling of NO and SO_2 without the need for scavengers.[114] The formation of the SO_2–NO redox pair facilitates high conversion rates of both NO and SO_2 in continuous flow. Achieving a remarkable selectivity for both NO-to-NH_3 upcycling (97%) and SO_2-to-SO_4^{2-} purification (92%) simultaneously underscores the practicability of value-added conversion of air pollutants (Fig. 7a and b).[114] Maintaining the efficiency of NO conversion and reduction crucially depends on preventing the oxidation of Fe(II) to Fe(III) in Fe(II) EDTA. Through verified *in situ* ATR-FTIR experiments, it was revealed that SO_2 exhibited a promoting effect on Fe(II) maintenance, while no interaction was observed between SO_2 and EDTA (Fig. 7c and d).

The chemical redox pair of SO_2–Fe(III) is illustrated in eqn (21)–(23).[114]

$$\text{Fe(II)} \rightarrow \text{Fe(III)} \text{ (spontaneous oxidation)} \tag{21}$$

$$SO_2 + H_2O \rightarrow SO_3^{2-} + 2H^+ \text{ (dissolution)} \tag{22}$$

$$2\text{Fe(III)} + 2SO_3^{2-} + O_2 \rightarrow 2\text{Fe(II)} + 2SO_4^{2-} \text{ (chemical redox pair)} \tag{23}$$

As depicted in Fig. 7e and f, compared to h^+-induced $^\bullet$OH production, the h^+-induced SO_2 oxidation reaction to $^\bullet SO_3^-$ promotes charge separation, thereby generating more e^-, and enhancing the efficiency of the nitrogen oxide reduction reaction to produce NH_3. The overall mechanism for synchronous NO and SO_2 conversion is illustrated in eqn (24)–(26):

$$SO_2 + H_2O \rightarrow SO_3^{2-} + 2H^+ \text{ (dissolution)} \tag{24}$$

$$5SO_3^{2-} + NO + 5h^+ + 5e^- + 5H^+ \rightarrow 5^\bullet SO_3^- + NH_4^+ + OH^- \text{ (photocatalytic redox pair)} \tag{25}$$

$$5^\bullet SO_3^- + NO + 5h^+ + 5e^- + 5H^+ + 9OH^- \rightarrow 5SO_4^{2-} + NH_4^+ + 5H_2O \text{ (photocatalytic redox pair)} \tag{26}$$

Thus, a one-step NO_x reduction method has been devised by concurrently absorbing and converting NO_x. This system also exhibits great resistance to toxicity, including resistance to K^+, Ca^{2+}, and Cd^{2+} metal ions, respectively. The effective separation and retrieval of reaction products provide this system with sustainable stability and potential economic viability. Continuous NO_x removal and upcycling under ambient conditions with high conversion efficiencies were achieved, marking significant advancements in photocatalytic NO_x removal and recycling compared to SCR and chemical absorption technologies.

4.2 Two-step method (NO → NO_3^- → NH_3)

Among the redox products of NO_x, NO_3^- is the dominant and accessible substance on the surface of the photocatalyst.[39,67]

Significant quantities of NO_3^- are released into the environment through processes such as the combustion of fossil fuels and agricultural activities, driven by the progress of urbanization and industrialization.[115] The surface of the photocatalyst is the overlooked storage site for NO_3^-, where the generated nitrate could be easily removed from the catalyst and subsequently concentrated in liquid form.[69,116] However, excessive amounts of NO_3^- in water can pose a pollution concern. To address this issue, photocatalytic technologies have been employed to convert excess nitrate into valuable NH_3.

Photocatalytic reduction of NO_3^- to ammonia *via* multiple electron transfer (eqn (27)), could emerge as a potent method for ammonia production under ambient conditions of room temperature and atmospheric pressure.[117] N_2 and H_2 formation reactions are two side reactions that consume photoexcited electrons (eqn (28) and (29)).[117,118] Therefore, it is necessary to enhance not only the ammonia yield but also the ammonia selectivity. A summary of studies on the reduction process of nitrate to ammonia by various photocatalysts is presented in Table 1.

$$NO_3^- + 9H^+ + 8e^- \rightarrow NH_3 + 3H_2O\ (1.20\ \text{V}\ \textit{vs.}\ \text{NHE}) \quad (27)$$

$$NO_3^- + 6H^+ + 5e^- \rightarrow 1/2N_2 + 3H_2O\ (1.25\ \text{V}\ \textit{vs.}\ \text{NHE}) \quad (28)$$

$$2H^+ + 2e^- \rightarrow H_2\ (0.00\ \text{V}\ \textit{vs.}\ \text{NHE}) \quad (29)$$

It can be inferred from Table 1 that TiO_2-based materials are prominently utilized as catalysts for NO_3^--to-NH_3 reduction, particularly highlighting metal-modified TiO_2 nanosheets (TNSs). Recently, as shown in Fig. 8a, alkaline-earth oxide clusters constructed on TiO_2 nanosheets (MO_{NCs}-TNSs, M = Mg, Ca, Sr or Ba) were reported to enhance NO_3^--to-NH_4^+ production, among which BaO_{NCs}-TNSs achieve both exceedingly high NH_4^+ selectivity (97.7%) and high NH_4^+ yield (89.8 mmol g_{cat}^{-1} h^{-1}).[121] To the best of our knowledge, this is the highest production of ammonia by the photocatalytic reduction reaction. Remarkably, there's an incremental rise in the rate of ammonia synthesis throughout the reaction, attributed to the concurrent Operando formation of BaO_{NCs} and the ammonia synthesis reaction (Fig. 8b and c). Upon achieving stabilization of BaO_{NCs} on TNSs, a notable and consistent production of ammonia on BaO_{NCs}-TNS composites was realized.

Chen *et al.*[119] further elucidated the criticality of the on-site formation of authentic active sites under realistic catalytic conditions. They engineered Cu_2O_{NCs}-TNS materials, wherein dynamic Cu_2O sub-nanoclusters were on-site constructed on TNSs using $CuCl_2$ solution through a photoinduced pseudo-Fehling's route. Different from BaO_{NCs}-TNS which remains stable once it has been constructed, the morphology and chemical state of Cu_2O exhibit dynamic evolution, as the actual reaction cannot progress over preformed Cu_2O sites (Fig. 8d and e). Numerous *in situ* experiments revealed a photoswitchable reversible conversion pattern between Cu^{2+} and Cu^+ in the photosynthesis reaction, aligning with the performance of ammonia synthesis by nitrate reduction (Fig. 8f and g).[119] NH_3 photosynthesis was directly attributed to the enhanced charge separation and transformation capacity from the Cu_2O active sites. Consequently, the establishment of a genuine structure–activity correlation was achieved by uncovering the synchronous formation of the Cu_2O active site and catalytic reaction (Fig. 8h).

In addition, a groundbreaking perspective has emerged regarding the interplay between single atoms and oxygen vacancies (OVs) (Fig. 9).[118] The incorporation of single-atom Cu into TiO_2 nanosheets (Cu-TNSs) resulted in a 62-fold increase in ammonia production compared to pristine TiO_2, with a selectivity of 97.6%. The introduction of Cu atoms, replacing Ti sites, induces the generation of OVs and lattice strain. NO_3^- preferentially adsorbs onto Ti atoms neighboring Cu atoms. The near-isolated Cu atoms and OVs facilitate multiple NO_3^- adsorptions at a single site, effectively inhibiting the release of NO_2^-

Table 1 Comparison of the results of NH_3 production with different photocatalysts

Photocatalysts	Hole scavengers	Light source	pH	NO_3^- conversion (%)	NH_4^+ production (mmol g_{cat}^{-1} h^{-1})	NH_4^+ selectivity (%)	Ref.
Cu_2O_{NCs}-TNS	Formaldehyde	300 W Xe lamp	N/A	94.2	42.6	98.6	119
CuO_x@TNS	Ethylene glycol	300 W Xe lamp	8.3	100	16	96.1	120
Cu-TNS	Formic acid	300 W Xe lamp	3.5–3.6	>99	0.1	97.6	118
BaO_{NCs}@TNS	Ethylene glycol	300 W Xe lamp	7	∼3.5	89.8	97.7	121
Photo-reductive TiO_2	N/A	450 W medium pressure UV	7	∼71	N/A	60	122
$LaFeO_3$/HTCC nanocomposites	Acetic acid	300 W Xe lamp	2	94.6	N/A	88.7	123
$LaFeO_3$/biochar nanocomposites	Formic acid	300 W Xe lamp	2	98	N/A	97	124
Ni/H_xWO_{3-y} hybrids	Ethylene glycol	300 W Xe lamp	N/A	∼92	10.5	98.3	125
Carbon/bismuth/Bi_2O_3	Ethylene glycol	Simulated sunlight	N/A	N/A	0.4	95	126
CuAg/TiO_2	Methanol	Black light	6	96	N/A	85	127
Ni_2P/Ta_3N_5	N/A	Fluorescent lamps	2	79	0.2	68	128
PdSn/NiO/$NaTaO_3$:La	Formic acid	125 W high pressure UV	N/A	100	N/A	72	129
JRC-TIO-6 (rutile TiO_2)	Formic acid	2 kW Xe lamp	2.4–3	79	0.02	97	117
CuPd/TiO_2	Methanol	UV	N/A	>95	N/A	78	130

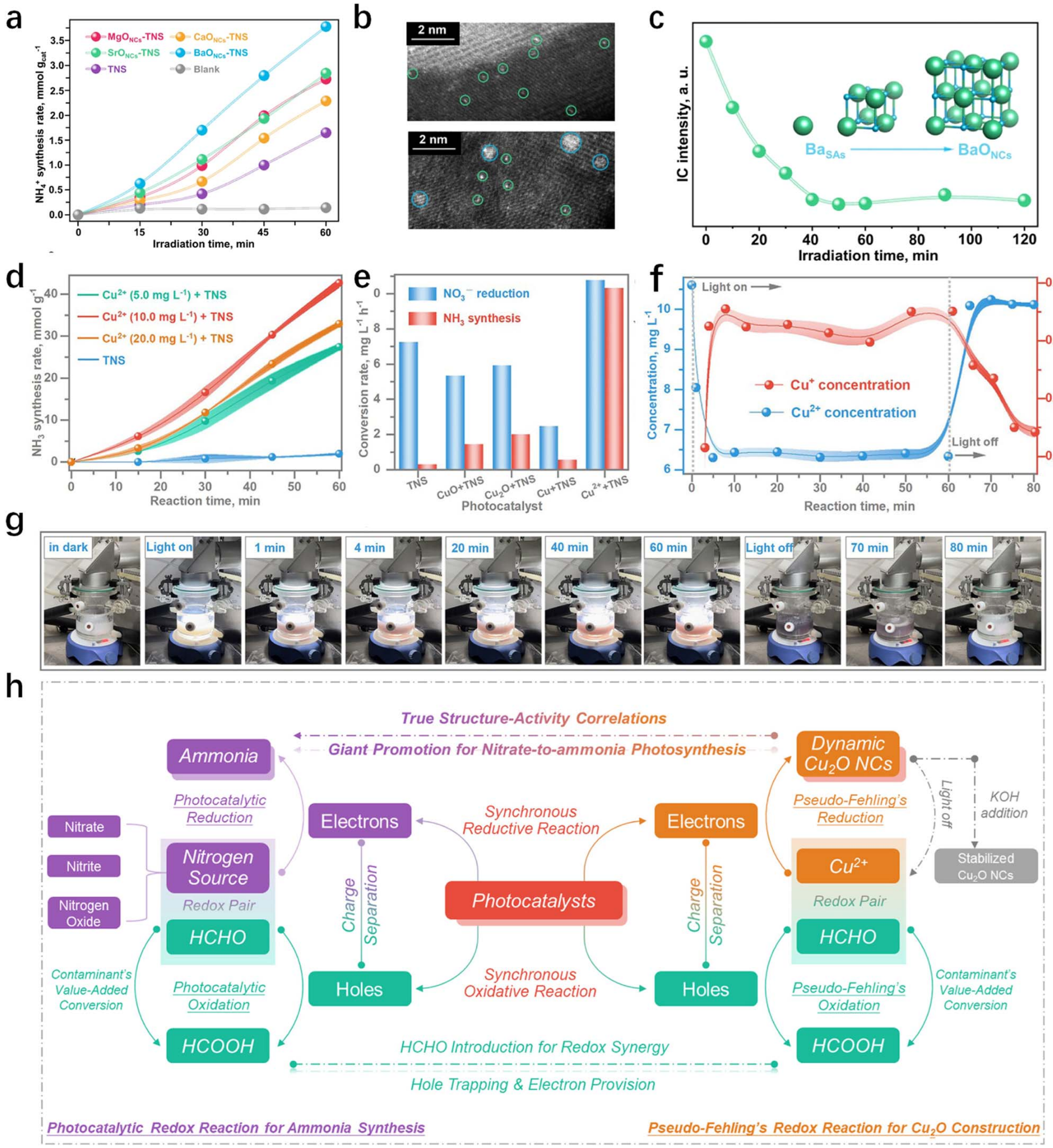

Fig. 8 (a) Catalytic efficiency tests showing the enhancement of Operando construction of alkaline-earth oxide clusters on TNS surfaces. (b) Quasi *in situ* high-angle annular dark-field scanning transmission electron microscopy (HAADF-STEM) images showing the evolution course from isolated Ba single atoms (Ba_{SAs}) to subnanometric (BaO_{NCs}) at the irradiation time of 5 min (up) and 10 min (down). (c) Variation of Ba^{2+} concentration during the Operando construction of BaO_{NCs} detected by ion chromatography.[121] (d) NH_3 photosynthesis rate of the dynamic process. (e) Efficiency comparison between the different composites of Cu species and the TNS substrate. (f) The evolution process of the different chemical states of Cu^{2+} and Cu^+ under the catalysis conditions. (g) Snapshots of the photosynthesis reactor along with the photosynthesis reaction time for the observation of the dynamic evolution of Cu species. (h) Schematic illustrations for the synchronous Cu_2O NCs construction and NH_3 photosynthesis in the realistic catalysis condition.[119]

intermediates and minimizing N-to-N interactions, thus ensuring high NH_3 selectivity.

Furthermore, CuO_x@TNS was designed for NO_3^- reduction with a 100% NO_3^- conversion rate and 96.1% ammonia selectivity by coupling the nitrate reduction reaction with a glycol oxidation reaction system.[120] The active site for improving ammonia formation is identified as the CuO_x species with an amorphous Cu–O–Ti bimetallic oxide cluster structure

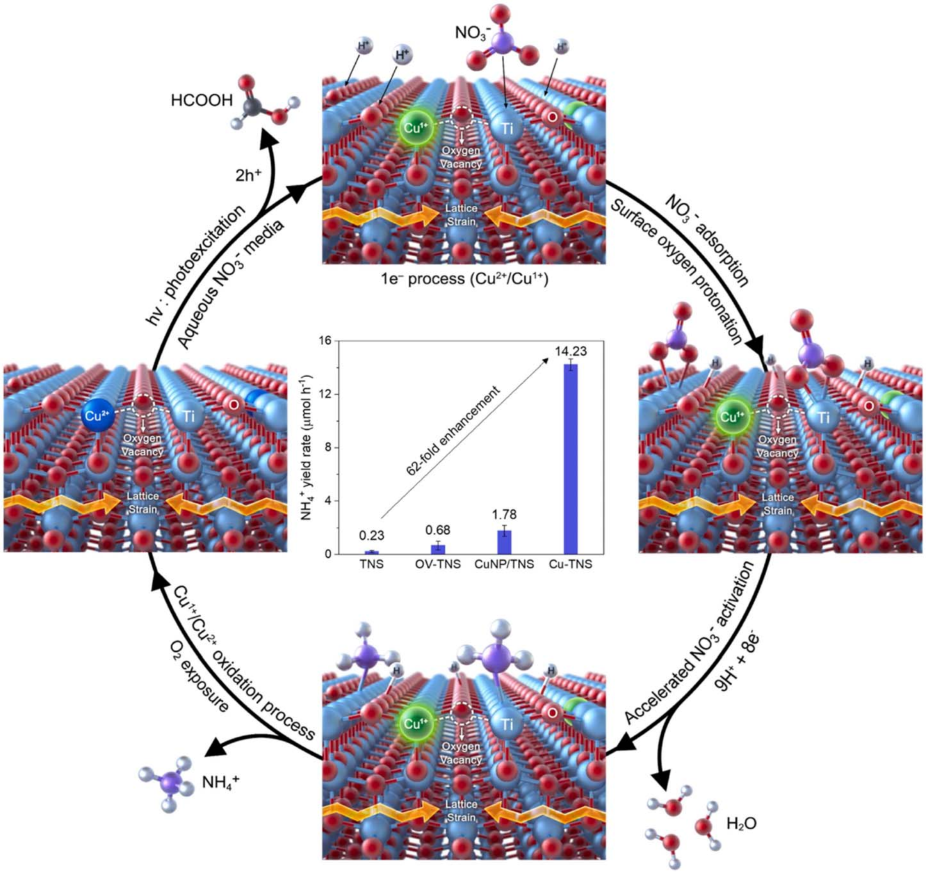

Fig. 9 NO$_3^-$-to-NH$_3$ reaction mechanism on Cu-TNSs. TiO$_2$ with isolated Cu^{2+} atomic sites (blue) and defects generates photoexcited electrons and holes under light irradiation.[118]

(Fig. 10a).[120] Given that redox reactions occur concurrently, it's evident that the oxidation half-reaction also significantly influences NH$_3$ production. To explore the impact of various oxidation half-reactions on NO$_3^-$ reduction, oxidative reactants including deionized water (DI), methanol (CH$_3$OH), ethylene glycol ((CH$_2$OH)$_2$), and acetic acid (HCOOH) are introduced into the reaction system (Fig. 10b and c). It is revealed that the NO$_3^-$ reduction process is hindered by the formation of potent oxidizing $^{\bullet}$OH radicals (Fig. 10d). The presence of ethylene glycol expedites the consumption of h$^+$ during the formation of alkoxy radicals ($^{\bullet}$R), thus mitigating $^{\bullet}$OH production. Moreover, the Cu–O–Ti sites could promote the preferential oxidation of ethylene glycol, thereby enhancing both the efficiency and selectivity of ammonia production (Fig. 10e). These findings underscore the pivotal role of the oxidation half-reaction. The deliberate design of the oxidation half-reaction not only enhances the effective utilization of electrons and holes but also modulates the reaction pathway, thus promoting the progress of the NO$_3^-$ reduction half-reaction.

In summary, the photocatalytic performance of NO$_3^-$-to-NH$_3$ photocatalytic reduction highly relies on the strategic construction of active sites and the coordination of redox reactions. This offers an innovative perspective on experimental design aimed at achieving high NH$_3$ selectivity and production. Recent studies have shown that NO$_3^-$ originating from NO oxidation has achieved nearly 100% NH$_3$ selectivity. It is desired to employ a two-step process (NO → NO$_3^-$ → NH$_3$) to achieve a highly selective conversion of NO to NH$_3$.

5 Conclusions and perspectives

5.1 Conclusions

Table 2 summarizes and compares the application scenarios, reaction conditions, photocatalysts, and reaction activity for NO$_x$ removal under the different reaction pathways. It is found that the application of photocatalytic technology has transcended indoor NO$_x$ treatment and is now addressing challenges posed by complex pollutant compositions and industrial flue gases. Interestingly, TiO$_2$ remains the most extensively studied photocatalyst in both NO$_x$ oxidation and NO$_x$ reduction, probably due to its outstanding carrier separation capability. Besides, the overall redox properties also depend on catalyst modification or adjustment of environmental atmospheres in different systems. The photocatalytic performance showed that the NO$_x$ conversion and product selectivity have exceeded 90% for most of the redox pathways except NO$_x$ decomposition. This marks a significant advancement towards the future application of photocatalytic NO$_x$ removal and recovery.

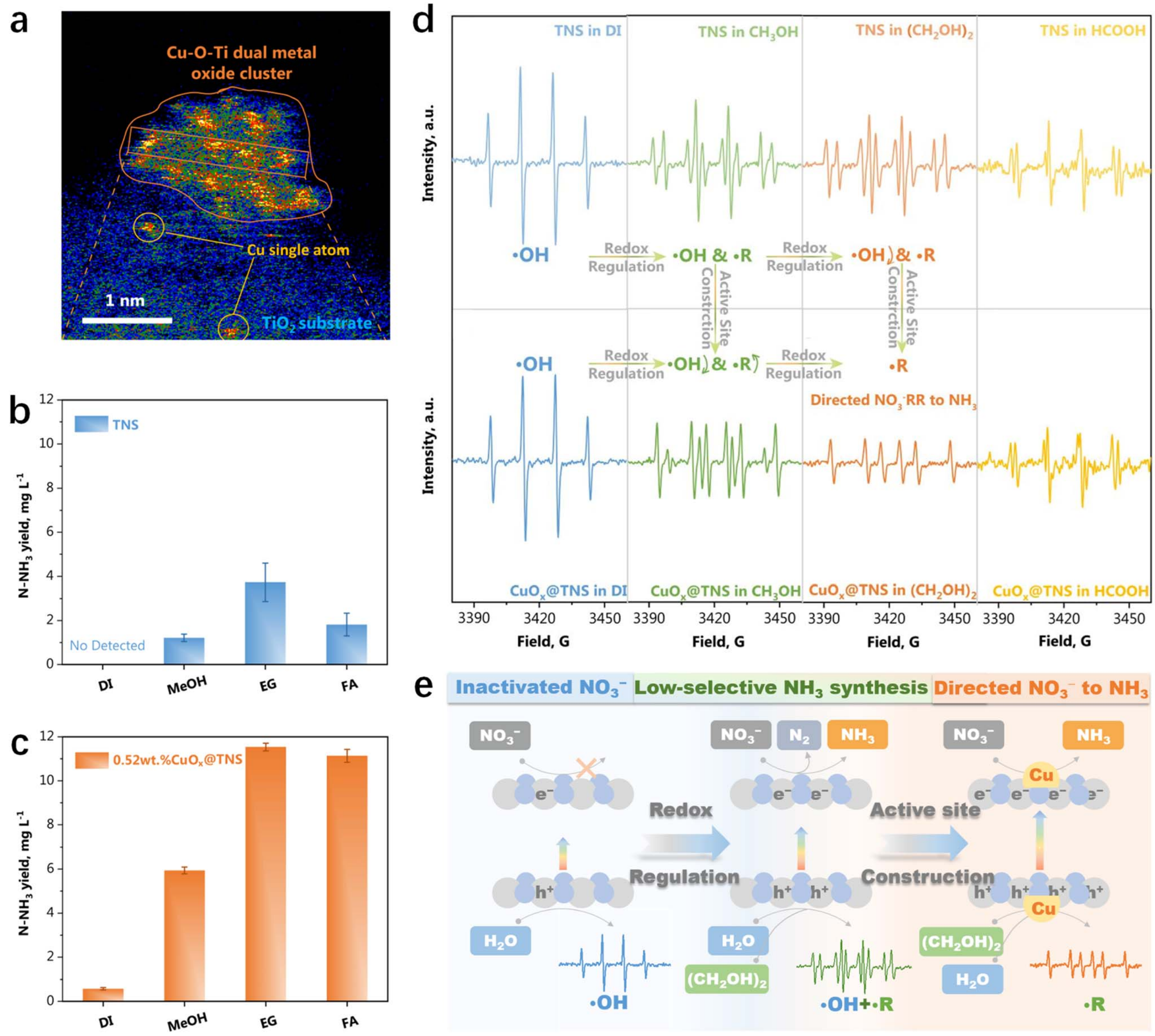

Fig. 10 (a) Magnified HAADF-STEM image of 0.52 wt% CuO$_x$@TNS. NH$_3$ photosynthesis yields under different cooperative oxidative half-reactions for (b) TNSs and (c) 0.52 wt% CuO$_x$@TNS after 1 h irradiation. (d) EPR spectra of DI, CH$_3$OH, (CH$_2$OH)$_2$, and HCOOH oxidative half-reactions on TNSs and 0.52 wt% CuO$_x$@TNS catalyst after light irradiation for 5 min. (e) Illustration of the directed NO$_3^-$RR by coordination of different oxidative reactions.[120]

In conclusion, photocatalytic technology is a promising method for NO$_x$ removal and recovery, owing to its mild reaction conditions and eco-friendliness. In recent years, significant strides have been made in the field of photocatalytic NO$_x$ removal, spanning from the optimization of photocatalysts to the exploration of mechanisms and the modulation of reaction pathways, resulting in unprecedented performance in NO$_x$ removal. The emerging photocatalytic reduction of NO$_x$ to ammonia offers a viable alternative for NO$_x$ recovery. This review summarizes the latest advancements in photocatalytic removal, encompassing NO$_x$ oxidation (both single and synergistic removal, as well as NO$_3^-$ decomposition), NO$_x$ reduction to nitrogen, and the upcycling of NO$_x$ into ammonia. Furthermore, we highlight photocatalysis-based NO$_x$ recovery, including one-step and two-step methods, as a promising approach to tackle existing environmental and energy challenges.

5.2 Future outlook

The utilization of photocatalytic technology for the removal and recovery of NO$_x$ is currently in the research phase, with the practical application still a considerable distance away. We recommend that future studies systematically address the following issues:

(1) Comparing the performance of photocatalysts across different studies in the realm of NO$_x$ oxidation proves

Table 2 Conclusion and comparison of NO_x removal by various reaction pathways

Reaction pathway		Product	Scenarios of application	Typical photocatalysts	NO_x concentration	Temperature (°C)	Flow rate ($L\ min^{-1}$)/ GHSV (h^{-1})	Carrier gas	Supplements	Conversion (%)	Selectivity (%)
NO_x oxidation	Single oxidation	NO_3^-	Air purification	TiO_2, g-C_3N_4, WO_3, Bi-based materials	~600 ppb	Room temperature	1 L min^{-1}	Air	N/A	~90	~97
	Mixed oxidation	NO_3^-	Air purification	TiO_2, $In(OH)_3$, $Sr_2Sb_2O_7$	30 ppm	Room temperature	1 L min^{-1}	Air	VOCs, SO_2	~100	N/A
NO_x reduction	NO_x decomposition	N_2	Air purification	TiO_2, g-C_3N_4	<1 ppm	N/A	1 L min^{-1}	Air/Ar	N/A	~50	N/A
	NO_x photo-SCR	N_2	Flue gas treatment	TiO_2, perovskite	1000 ppm	<200	50 000 h^{-1}	3% O_2, 97% N_2	NH_3, H_2, hydrocarbon, *etc.*	>90	~100
NO_x upcycling	One-step method	NH_3	Flue gas treatment	TiO_2	500 ppm	25	25 000 h^{-1}	N/A	Fe(II)EDTA/hole scavengers (*e.g.* HCHO, SO_2)	97.6	~97.1%

challenging due to the diverse array of reaction conditions such as light source, gas flow rate, initial NO_x concentration, mass of the photocatalyst, reactor design, and others. To comprehensively evaluate photocatalyst performance and identify truly efficient photocatalysts, there is a pressing need to establish uniform performance standards.

(2) Despite notable advancements in the performance of photocatalytic NO_x removal in recent years, a gap persists when compared to thermal catalytic NO_x removal. One of the primary reasons for this gap is the insufficient exploration of the interfacial reaction mechanism governing photocatalytic NO_x removal. To address this, *in situ* detection methods with higher resolution, such as *in situ* EPR, DRIFTS, and Raman spectroscopy, should be more extensively employed. These techniques can unveil the intricacies of the photocatalytic reaction mechanism, subsequently informing catalyst design and modification efforts.

(3) In the one-step method, the yield of ammonia is significantly influenced by the solubility of NO, thus necessitating further enhancement of NO solubility in water. Introducing chemical absorbents to adsorb NO suggests the need for additional methods to separate the resulting ammonia, thereby increasing costs and rendering it less favorable for practical applications. An absorbent-free approach is preferable to augment the solubility of high concentrations of NO in water and to develop photocatalysts capable of achieving an ammonia yield that meets recovery criteria. Moreover, photocatalysts can be selectively designed to further reduce NO_x to N_2 instead of ammonia, offering an alternative solution to address current environmental challenges.

(4) In the two-step process, the primary challenge lies in effectively collecting the nitrates produced from NO_x. During the photocatalytic NO_x oxidation process, nitrates gradually accumulate on the catalyst surface. However, due to the limited availability of adsorption sites on the surface and the simultaneous decomposition of nitrates, only a small portion of nitrates remains on the photocatalyst surface. It is imperative to enhance the thorough oxidation of NO_x and suppress the decomposition of nitrates. Additionally, nitrates are commonly found in relatively high concentrations in wastewater, presenting an opportunity to enhance ammonia production.

(5) Machine learning offers a potent tool for predicting catalytic reaction performance accurately, aiding chemists in tasks like material screening, experiment optimization, and mechanistic studies. Nonetheless, it's crucial to emphasize that machine learning should be applied judiciously. While it's a valuable tool, it's not a universal solution and cannot substitute well-considered experimental designs. In practice, a combination of expertise is still vital to ensure that machine learning and traditional methods work together harmoniously to achieve broader environmental science objectives.

Author contributions

All of the authors contributed to the literature search, writing and editing of this review.

Conflicts of interest

There are no conflicts to declare.

Acknowledgements

This work was supported by the National Natural Science Foundation of China (22261142663, 22225606, and 22176029).

References

1 J. Lelieveld, J. S. Evans, M. Fnais, D. Giannadaki and A. Pozzer, The contribution of outdoor air pollution sources to premature mortality on a global scale, *Nature*, 2015, **525**, 367–371.
2 S. C. Anenberg, J. Miller, R. Minjares, L. Du, D. K. Henze, F. Lacey, C. S. Malley, L. Emberson, V. Franco, Z. Klimont and C. Heyes, Impacts and mitigation of excess diesel-related NO_x emissions in 11 major vehicle markets, *Nature*, 2017, **545**, 467–471.
3 D. Shindell, G. Faluvegi, M. Walsh, S. C. Anenberg, R. Van Dingenen, N. Z. Muller, J. Austin, D. Koch and G. Milly, Climate, health, agricultural and economic impacts of tighter vehicle-emission standards, *Nat. Clim. Change*, 2011, **1**, 59–66.
4 N. Li, C. Wang, K. Zhang, H. Lv, M. Yuan and D. W. Bahnemann, Progress and prospects of photocatalytic conversion of low-concentration NO_x, *Chin. J. Catal.*, 2022, **43**, 2363–2387.
5 M. G. Lawrence and P. J. Crutzen, Influence of NO_x emissions from ships on tropospheric photochemistry and climate, *Nature*, 1999, **402**, 167–170.
6 J. Lasek, Y. H. Yu and J. C. S. Wu, Removal of NO_x by photocatalytic processes, *J. Photochem. Photobiol., C*, 2013, **14**, 29–52.
7 V. Smil, Detonator of the population explosion, *Nature*, 1999, **400**, 415.
8 S. Su, Y. Liang, G. Yin, Q. Wang, Y. Cai, X. Peng, M. N. Pervez and L. Lin, Anhydrous dyeing processes of ramie fiber in liquid ammonia, *Cellulose*, 2019, **26**, 8109–8120.
9 T. Wu, X. Zhu, Z. Xing, S. Mou, C. Li, Y. Qiao, Q. Liu, Y. Luo, X. Shi, Y. Zhang and X. Sun, Greatly Improving Electrochemical N_2 Reduction over TiO_2 Nanoparticles by Iron Doping, *Angew. Chem., Int. Ed.*, 2019, **58**, 18449–18453.
10 R. Schlögl, Catalytic Synthesis of Ammonia—A "Never-Ending Story", *Angew. Chem., Int. Ed.*, 2003, **42**, 2004–2008.
11 J. Egerer, V. Grimm, K. Niazmand and P. Runge, The economics of global green ammonia trade - "Shipping Australian wind and sunshine to Germany", *Appl. Energy*, 2023, **334**, 120662.
12 Q. An, M. McDonald, A. Fortunelli and W. A. Goddard III, Si-Doped Fe Catalyst for Ammonia Synthesis at Dramatically Decreased Pressures and Temperatures, *J. Am. Chem. Soc.*, 2020, **142**, 8223–8232.
13 X. Guo, P. Wang, T. Wu, Z. Wang, J. Li, K. Liu, J. Fu, M. Liu, J. Wu, Z. Lin, L. Chai, Z. Bian, H. Li and M. Liu, Aqueous Electroreduction of Nitric Oxide to Ammonia at Low Concentration via Vacancy Engineered FeOCl, *Angew. Chem., Int. Ed.*, 2023, e202318792.
14 K. A. Brown, D. F. Harris, M. B. Wilker, A. Rasmussen, N. Khadka, H. Hamby, S. Keable, G. Dukovic, J. W. Peters, L. C. Seefeldt and P. W. King, Light-driven dinitrogen reduction catalyzed by a CdS: nitrogenase MoFe protein biohybrid, *Science*, 2016, **352**, 448–450.
15 Q. Guo, Z. B. Ma, C. Y. Zhou, Z. F. Ren and X. M. Yang, Single Molecule Photocatalysis on TiO_2 Surfaces, *Chem. Rev.*, 2019, **119**, 11020–11041.
16 T. Wu, X. J. Liu, Y. Liu, M. Cheng, Z. F. Liu, G. M. Zeng, B. B. Shao, Q. H. Liang, W. Zhang, Q. Y. He and W. Zhang, Application of QD-MOF composites for photocatalysis: Energy production and environmental remediation, *Coord. Chem. Rev.*, 2020, **403**, 213097.
17 F. He, S. Weon, W. Jeon, M. W. Chung and W. Choi, Self-wetting triphase photocatalysis for effective and selective removal of hydrophilic volatile organic compounds in air, *Nat. Commun.*, 2021, **12**, 6259.
18 S. Wang, W. Cui, B. Lei, X. A. Dong, Y. Tang and F. Dong, Targeted NO Oxidation and Synchronous NO_2 Inhibition via Oriented $^1O_2$ Formation Based on Lewis Acid Site Adjustment, *Environ. Sci. Technol.*, 2023, **57**, 12890–12900.
19 R. Hailili, Z.-Q. Wang, H. Ji, C. Chen, X.-Q. Gong, H. Sheng and J. Zhao, Mechanistic insights into the photocatalytic reduction of nitric oxide to nitrogen on oxygen-deficient quasi-two-dimensional bismuth-based perovskites, *Environ. Sci.: Nano*, 2022, **9**, 1453–1465.
20 J. C.-C. Yu, V.-H. Nguyen, J. Lasek and J. C. S. Wu, Titania nanosheet photocatalysts with dominantly exposed (001) reactive facets for photocatalytic NO_x abatement, *Appl. Catal., B*, 2017, **219**, 391–400.
21 V.-H. Nguyen, B.-S. Nguyen, C.-W. Huang, T.-T. Le, C. C. Nguyen, T. T. Nhi Le, D. Heo, Q. V. Ly, Q. T. Trinh, M. Shokouhimehr, C. Xia, S. S. Lam, D.-V. N. Vo, S. Y. Kim and Q. V. Le, Photocatalytic NO_x abatement: Recent advances and emerging trends in the development of photocatalysts, *J. Cleaner Prod.*, 2020, **270**, 121912.
22 X. Shi, P. Wang, W. Li, Y. Bai, H. Xie, Y. Zhou and L. Ye, Change in photocatalytic NO removal mechanisms of ultrathin BiOBr/BiOI via NO_3^- adsorption, *Appl. Catal., B*, 2019, **243**, 322–329.
23 K. Li, H. Wang, J. Li and F. Dong, Design and mechanism of photocatalytic oxidation for the removal of air pollutants: a review, *Environ. Chem. Lett.*, 2022, **20**, 2687–2708.
24 Q. Li, J. Zhao, H. Shang, Z. Ma, H. Cao, Y. Zhou, G. Li, D. Zhang and H. Li, Singlet Oxygen and Mobile Hydroxyl Radicals Co-operating on Gas-Solid Catalytic Reaction Interfaces for Deeply Oxidizing NO_x, *Environ. Sci. Technol.*, 2022, **56**, 5830–5839.
25 A. Martinez-Oviedo, Y. K. Kshetri, B. Joshi and S. W. Lee, Surface modification of blue TiO_2 with silane coupling agent for NO_x abatement, *Prog. Nat. Sci.: Mater. Int.*, 2021, **31**, 230–238.
26 Y. Bu, B. Wang, M. Yue, Q. Ren, L. Guo and Y. Fu, Photocatalytic NO removal based on TiO_2 photonic

crystals through slow photon effect, *Mater. Lett.*, 2023, **346**, 134537.

27 M. Kamran, T. A. Kandiel, S. Abdel-Azeim, M. A. Morsy and D. W. Bahnemann, Mechanistic Insights into the High Selectivity and Photocatalytic Activity of Brookite TiO_2 toward NO_x Abatement, *J. Phys. Chem. C*, 2023, **127**, 7707–7717.

28 Y. Xin, Q. Zhu, T. Gao, X. Li, W. Zhang, H. Wang, D. Ji, Y. Huang, M. Padervand, F. Yu and C. Wang, Photocatalytic NO removal over defective Bi/BiOBr nanoflowers: The inhibition of toxic NO_2 intermediate via high humidity, *Appl. Catal., B*, 2023, **324**, 122238.

29 Q. Zhu, Y. Wang, J. Wang, J. Luo, J. Xu and C. Wang, Synergistic polarization and oxygen vacancies engineering for enhancing photocatalytic NO removal over $Bi_4Ti_3O_{12}$ nanowires, *Appl. Catal., B*, 2024, **346**, 123734.

30 Y. Shi, Z. Yang, L. Shi, H. Li, X. Liu, X. Zhang, J. Cheng, C. Liang, S. Cao, F. Guo, X. Liu, Z. Ai and L. Zhang, Surface Boronizing Can Weaken the Excitonic Effects of BiOBr Nanosheets for Efficient O_2 Activation and Selective NO Oxidation under Visible Light Irradiation, *Environ. Sci. Technol.*, 2022, **56**, 14478–14486.

31 D. Liu, D. Chen, N. Li, Q. Xu, H. Li, J. He and J. Lu, Surface Engineering of g-C_3N_4 by Stacked BiOBr Sheets Rich in Oxygen Vacancies for Boosting Photocatalytic Performance, *Angew. Chem., Int. Ed.*, 2020, **59**, 4519–4524.

32 Y. Geng, D. Chen, N. Li, Q. Xu, H. Li, J. He and J. Lu, Z-Scheme 2D/2D α-Fe_2O_3/g-C_3N_4 heterojunction for photocatalytic oxidation of nitric oxide, *Appl. Catal., B*, 2021, **280**, 119409.

33 Z. Chen, H. Yin, R. Wang, Y. Peng, C. You and J. Li, Efficient Electron Transfer by Plasmonic Silver in $SrTiO_3$ for Low-Concentration Photocatalytic NO Oxidation, *Environ. Sci. Technol.*, 2022, **56**, 3604–3612.

34 H. Shang, H. Jia, P. Li, H. Li, W. Zhang, S. Li, Q. Wang, S. Xiao, D. Wang, G. Li and D. Zhang, Highly selective and efficient photocatalytic NO removal: Charge carrier kinetics and interface molecular process, *J. Nano Res.*, 2024, **17**, 1003–1026.

35 G. Liu, Y. Huang, H. Lv, H. Wang, Y. Zeng, M. Yuan, Q. Meng and C. Wang, Confining single-atom Pd on g-C_3N_4 with carbon vacancies towards enhanced photocatalytic NO conversion, *Appl. Catal., B*, 2021, **284**, 119683.

36 L. Hu, J. Liu, X. Huang, Q. Nie, P. Liu, Z. Tan and H. Yu, Carbon-bridged atomically dispersed platinum on MOF-derived ZnO/C for selective photocatalytic oxidation of NO into Nitrates and Nitrites, *Carbon*, 2023, **214**, 118299.

37 R. Zhang, Y. Cao, D. E. Doronkin, M. Ma, F. Dong and Y. Zhou, Single-atom dispersed Zn-N_3 active sites bridging the interlayer of g-C_3N_4 to tune NO oxidation pathway for the inhibition of toxic by-product generation, *Chem. Eng. J.*, 2023, **454**, 140084.

38 Z. Hu, X. Li, S. Zhang, Q. Li, J. Fan, X. Qu and K. Lv, Fe_1/TiO_2 Hollow Microspheres: Fe and Ti Dual Active Sites Boosting the Photocatalytic Oxidation of NO, *Small*, 2020, **16**, 2004583.

39 F. Guo, C. Mao, C. Liang, P. Xing, L. Yu, Y. Shi, S. Cao, F. Wang, X. Liu, Z. Ai and L. Zhang, Triangle Cl-Ag_1-Cl Sites for Superior Photocatalytic Molecular Oxygen Activation and NO Oxidation of BiOCl, *Angew. Chem., Int. Ed.*, 2023, e202314243.

40 A. M. Żurański, J. I. Martinez Alvarado, B. J. Shields and A. G. Doyle, Predicting Reaction Yields via Supervised Learning, *Acc. Chem. Res.*, 2021, **54**, 1856–1865.

41 S. Zhong, K. Zhang, M. Bagheri, J. G. Burken, A. Gu, B. Li, X. Ma, B. L. Marrone, Z. J. Ren, J. Schrier, W. Shi, H. Tan, T. Wang, X. Wang, B. M. Wong, X. Xiao, X. Yu, J.-J. Zhu and H. Zhang, Machine Learning: New Ideas and Tools in Environmental Science and Engineering, *Environ. Sci. Technol.*, 2021, **55**, 12741–12754.

42 J. Li, X. Liu, H. Wang, Y. Sun and F. Dong, Prediction and interpretation of photocatalytic NO removal on g-C_3N_4-based catalysts using machine learning, *Chin. Chem. Lett.*, 2024, **35**, 108596.

43 B. J. Finlayson-Pitts and J. N. Pitts, *Chemistry of the Upper and Lower Atmosphere: Theory, Experiments, and Applications*, 1999.

44 Y. Cao, Q. Ma, B. Chu and H. He, Homogeneous and heterogeneous photolysis of nitrate in the atmosphere: state of the science, current research needs, and future prospects, *Front. Environ. Sci. Eng.*, 2023, **17**(4), 48.

45 J. Schuttlefield, G. Rubasinghege, M. El-Maazawi, J. Bone and V. H. Grassian, Photochemistry of adsorbed nitrate, *J. Am. Chem. Soc.*, 2008, **130**, 12210.

46 X. L. Zhou, H. L. Gao, Y. He, G. Huang, S. B. Bertman, K. Civerolo and J. Schwab, Nitric acid photolysis on surfaces in low-NO_x environments: Significant atmospheric implications, *Geophys. Res. Lett.*, 2003, **30**, 2217.

47 H. Wang, Y. Sun and F. Dong, Insight into the Overlooked Photochemical Decomposition of Atmospheric Surface Nitrates Triggered by Visible Light, *Angew. Chem., Int. Ed.*, 2022, **61**, e202209201.

48 Q. W. Shi, Y. Tao, J. E. Krechmer, C. L. Heald, J. G. Murphy, J. H. Kroll and Q. Ye, Laboratory Investigation of Renoxification from the Photolysis of Inorganic Particulate Nitrate, *Environ. Sci. Technol.*, 2021, **55**, 854–861.

49 C. Ye, X. Zhou, D. Pu, J. Stutz, J. Festa, M. Spolaor, C. Tsai, C. Cantrell, R. L. Mauldin III, T. Campos, A. Weinheimer, R. S. Hornbrook, E. C. Apel, A. Guenther, L. Kaser, B. Yuan, T. Karl, J. Haggerty, S. Hall, K. Ullmann, J. N. Smith, J. Ortega and C. Knote, Rapid cycling of reactive nitrogen in the marine boundary layer, *Nature*, 2016, **532**, 489–491.

50 H. Schwartz-Narbonne, S. H. Jones and D. J. Donaldson, Indoor Lighting Releases Gas Phase Nitrogen Oxides from Indoor Painted Surfaces, *Environ. Sci. Technol. Lett.*, 2019, **6**, 92–97.

51 F. Karagulian, C. Santschi and M. J. Rossi, The heterogeneous chemical kinetics of N_2O_5 on $CaCO_3$ and other atmospheric mineral dust surrogates, *Atmos. Chem. Phys.*, 2006, **6**, 1373–1388.

52 M. Ndour, P. Conchon, B. D'Anna, O. Ka and C. George, Photochemistry of mineral dust surface as a potential atmospheric renoxification process, *Geophys. Res. Lett.*, 2009, **36**, L05816.

53 Y. Bedjanian and A. El Zein, Interaction of NO_2 with TiO_2 Surface Under UV Irradiation: Products Study, *J. Phys. Chem. A*, 2012, **116**, 1758–1764.

54 G. Rubasinghege and V. H. Grassian, Photochemistry of Adsorbed Nitrate on Aluminum Oxide Particle Surfaces, *J. Phys. Chem. A*, 2009, **113**, 7818–7825.

55 Y. Liu, X. Wang, J. Shang, W. Xu, M. Sheng and C. Ye, The positive effect of formaldehyde on the photocatalytic renoxitication of nitrate on TiO_2 particles, *Atmos. Chem. Phys.*, 2022, **22**, 11347–11358.

56 M. S. Rosseler, V. Nahuel Montesinos, A. Shavorskiy, V. Keller, N. Keller, M. I. Litter, H. Bluhm, M. Salmeron and H. Destaillats, Chemistry of NO_x on TiO_2 Surfaces Studied by Ambient Pressure XPS: Products, Effect of UV Irradiation, Water, and Coadsorbed K^+, *J. Phys. Chem. Lett.*, 2013, **4**, 536–541.

57 Q. Ma, C. Zhong, J. Ma, C. Ye, Y. Zhao, Y. Liu, P. Zhang, T. Chen, C. Liu, B. Chu and H. He, Comprehensive Study about the Photolysis of Nitrates on Mineral Oxides, *Environ. Sci. Technol.*, 2021, **55**, 8604–8612.

58 H. Shang, Z. Chen, X. Wang, M. Li, H. Li, C. Mao, L. Yu, J. Sun, Z. Ai and L. Zhang, SO_2-enhanced nitrate photolysis on TiO_2 minerals: A vital role of photochemically reactive holes, *Appl. Catal., B*, 2022, **308**, 121217.

59 H. Wang, K. Li, J. Li, Y. Sun and F. Dong, Photochemical Transformation Pathways of Nitrates from Photocatalytic NO_x Oxidation: Implications for Controlling Secondary Pollutants, *Environ. Sci. Technol. Lett.*, 2021, **8**, 873–877.

60 M. S. Gen, R. F. Zhang, D. D. Huang, Y. J. Li and C. K. Chan, Heterogeneous Oxidation of SO_2 in Sulfate Production during Nitrate Photolysis at 300 nm: Effect of pH, Relative Humidity, Irradiation Intensity, and the Presence of Organic Compounds, *Environ. Sci. Technol.*, 2019, **53**, 8757–8766.

61 J. N. Pitts, A. M. Winer, R. Atkinson and W. P. Carter, Comment on "Effect of nitrogen oxide emissions on ozone levels in metropolitan regions", "Effect of nitrogen oxide (NO_x) emission rates on smog formation in the California South Coast Air Basin", and "Effect of hydrocarbon and nitrogen oxide (NO_x) on photochemical smog formation under simulated transport conditions, *Environ. Sci. Technol.*, 1983, **17**, 54–57.

62 Y. Qiu, Z. Ma, K. Li, W. Lin, Y. Tang, F. Dong and H. Liao, Markedly Enhanced Levels of Peroxyacetyl Nitrate (PAN) During COVID-19 in Beijing, *Geophys. Res. Lett.*, 2020, **47**, e2020GL089623.

63 C. Li, Q. Zhu, X. Jin and R. C. Cohen, Elucidating Contributions of Anthropogenic Volatile Organic Compounds and Particulate Matter to Ozone Trends over China, *Environ. Sci. Technol.*, 2022, 12906–12916.

64 A. Mellouki, T. J. Wallington and J. Chen, Atmospheric Chemistry of Oxygenated Volatile Organic Compounds: Impacts on Air Quality and Climate, *Chem. Rev.*, 2015, **115**, 3984–4014.

65 Z. Meng, D. Dabdub and J. H. Seinfeld, Chemical coupling between atmospheric ozone and particulate matter, *Science*, 1997, **277**, 116–119.

66 Z. Chen, H. Yin, C. Wang, R. Wang, Y. Peng, C. You and J. Li, New Insights on Competitive Adsorption of NO/SO_2 on TiO_2 Anatase for Photocatalytic NO Oxidation, *Environ. Sci. Technol.*, 2021, **55**, 9285–9292.

67 T. Xue, L. Chen, K. Li, B. Lei, H. Wang, F. Dong and Y. Yang, Highly Enhanced Photocatalytic NO Removal and Inhibited Peroxyacetyl Nitrate Formation in Synergistic Acetaldehyde Degradation, *Environ. Sci. Technol.*, 2023, **57**, 8174–8182.

68 K. Li, H. Wang, L. Chen, J. Li and F. Dong, Synergistic degradation of NO and C_7H_8 for inhibition of O_3 generation, *Appl. Catal., B*, 2022, **312**, 121423.

69 K. Li, T. Xue, L. Chen, J. Li, F. Dong and Y. Sun, Dual function of H_2O on interfacial intermediate conversion and surface poisoning regulation in simultaneous photodegradation of NO and toluene, *Environ. Res.*, 2024, **240**, 117526.

70 X. Wang, A. Mahmood, G. Lu, X. Xie and J. Sun, Synergistic photocatalytic treatment of aromatic hydrocarbons/NO_x mixtures over TiO_2: The activation and replenishment of lattice oxygen, *Chem. Eng. J.*, 2022, **450**, 138168.

71 C. H. Ao, S. C. Lee, S. C. Zou and C. L. Mak, Inhibition effect of SO_2 on NO_x and VOC_s during the photodegradation of synchronous indoor air pollutants at parts per billion (ppb) level by TiO_2, *Appl. Catal., B*, 2004, **49**, 187–193.

72 M. Anpo, S. G. Zhang, H. Mishima, M. Matsuoka and H. Yamashita, Design of photocatalysts encapsulated within the zeolite framework and cavities for the decomposition of NO into N_2 and O_2 at normal temperature, *Catal. Today*, 1997, **39**, 159–168.

73 J. L. Zhang, Y. Hu, M. Matsuoka, H. Yamashita, M. Minagawa, H. Hidaka and M. Anpo, Relationship between the local structures of titanium oxide photocatalysts and their reactivities in the decomposition of NO, *J. Phys. Chem. B*, 2001, **105**, 8395–8398.

74 M. Anpo, M. Matsuoka, H. Yamashita, W. S. Ju, S. E. Park and Y. G. Shul, Photocatalytic decomposition of NO on transition metal ion-exchanged zeolite catalysts, *J. Ind. Eng. Chem.*, 2000, **6**, 133–143.

75 Y. Hu, S. Higashimoto, G. Martra, J. L. Zhang, M. Matsuoka, S. Coluccia and M. Anpo, Local structures of active sites on Ti-MCM-41 and their photocatalytic reactivity for the decomposition of NO, *Catal. Lett.*, 2003, **90**, 161–163.

76 Y. Hu, G. Martra, J. L. Zhang, S. Higashimoto, S. Coluccia and M. Anpo, Characterization of the local structures of Ti-MCM-41 and their photocatalytic reactivity for the decomposition of NO into N_2 and O_2, *J. Phys. Chem. B*, 2006, **110**, 1680–1685.

77 P. Y. Dong, N. Xu, Y. Xu and X. F. Wang, A study of Pt/WO_3-carrier catalysts for photocatalytic purification of NO gas, *Catal. Commun.*, 2016, **84**, 142–146.

78 N. Bowering, G. S. Walker and P. G. Harrison, Photocatalytic decomposition and reduction reactions of

nitric oxide over Degussa P25, *Appl. Catal., B*, 2006, **62**, 208–216.

79 M. Anpo, M. Takeuchi, K. Ikeue and S. Dohshi, Design and development of titanium oxide photocatalysts operating under visible and UV light irradiation.: The applications of metal ion-implantation techniques to semiconducting TiO_2 and Ti/zeolite catalysts, *Curr. Opin. Solid State Mater. Sci.*, 2002, **6**, 381–388.

80 M. Anpo and M. Takeuchi, Design and development of second-generation titanium oxide photocatalysts to better our environment-approaches in realizing the use of visible light, *Int. J. Photoenergy*, 2001, **3**, 90–94.

81 M. Xu, Y. Wang, J. Geng and D. Jing, Photodecomposition of NO_x on Ag/TiO_2 composite catalysts in a gas phase reactor, *Chem. Eng. J.*, 2017, **307**, 181–188.

82 Q. Wu and R. van de Krol, Selective Photoreduction of Nitric Oxide to Nitrogen by Nanostructured TiO_2 Photocatalysts: Role of Oxygen Vacancies and Iron Dopant, *J. Am. Chem. Soc.*, 2012, **134**, 9369–9375.

83 M. Anpo, T.-H. Kim and M. Matsuoka, The design of Ti-, V-, Cr-oxide single-site catalysts within zeolite frameworks and their photocatalytic reactivity for the decomposition of undesirable molecules—The role of their excited states and reaction mechanisms, *Catal. Today*, 2009, **142**, 114–124.

84 R. Hailili, Z. Q. Wang, H. W. Ji, C. C. Chen, X. Q. Gong, H. Sheng and J. C. Zhao, Mechanistic insights into the photocatalytic reduction of nitric oxide to nitrogen on oxygen-deficient quasi-two-dimensional bismuth-based perovskites, *Environ. Sci.: Nano*, 2022, **9**, 1453–1465.

85 L. Han, S. Cai, M. Gao, J.-Y. Hasegawa, P. Wang, J. Zhang, L. Shi and D. Zhang, Selective Catalytic Reduction of NO_x with NH_3 by Using Novel Catalysts: State of the Art and Future Prospects, *Chem. Rev.*, 2019, **119**, 10916–10976.

86 D. Wang, Q. Chen, X. Zhang, C. Gao, B. Wang, X. Huang, Y. Peng, J. Li, C. Lu and J. Crittenden, Multipollutant Control (MPC) of Flue Gas from Stationary Sources Using SCR Technology: A Critical Review, *Environ. Sci. Technol.*, 2021, **55**, 2743–2766.

87 X. Li, X. Yan, S. Zuo, X. Lu, S. Luo, Z. Li, C. Yao and C. Ni, Construction of $LaFe_{1-x}Mn_xO_3$/attapulgite nanocomposite for photo-SCR of NO_x at low temperature, *Chem. Eng. J.*, 2017, **320**, 211–221.

88 L. Ma, J. Li, Y. Cheng, C. K. Lambert and L. Fu, Propene Poisoning on Three Typical Fe-zeolites for SCR of NO_x with NH_3: From Mechanism Study to Coating Modified Architecture, *Environ. Sci. Technol.*, 2012, **46**, 1747–1754.

89 K. Teramura, T. Tanaka, S. Yamazoe, K. Arakaki and T. Funabiki, Kinetic study of photo-SCR with NH_3 over TiO_2, *Appl. Catal., B*, 2004, **53**, 29–36.

90 T. Tanaka, K. Teramura, T. Yamamoto, S. Takenaka, S. Yoshida and T. Funabiki, TiO_2/SiO_2 photocatalysts at low levels of loading: preparation, structure and photocatalysis, *J. Photochem. Photobiol., A*, 2002, **148**, 277–281.

91 Y.-C. Chou and Y. Ku, Preparation of high-aspect-ratio TiO_2 nanotube arrays for the photocatalytic reduction of NO in air streams, *Chem. Eng. J.*, 2013, **225**, 734–743.

92 R. Yuan, M. Wang, L. Liao, W. Hu, Z. Liu, Z. Liu, L. Guo, K. Li, Y. Cui, F. Lin, F. Tao and W. Zhou, 100% N_2O inhibition in photocatalytic NO_x reduction by carbon particles over Bi_2WO_6/TiO_2 Z-scheme heterojunctions, *Chem. Eng. J.*, 2023, **453**, 139892.

93 Y. Ren, Q. Han, J. Yang, Y. Zhao, Y. Xie, H. Wen and Z. Jiang, A promising catalytic solution of NO reduction by CO using $g\text{-}C_3N_4/TiO_2$: A DFT study, *J. Colloid Interface Sci.*, 2022, **610**, 152–163.

94 J. Lasek, Y.-H. Yu and J. C. S. Wu, Water and temperature effects on photo-selective catalytic reduction of nitric oxide on Pd-loaded TiO_2 photocatalyst, *Environ. Technol.*, 2012, **33**, 2133–2141.

95 R. Jin, Z. Wu, Y. Liu, B. Jiang and H. Wang, Photocatalytic reduction of NO with NH_3 using Si-doped TiO_2 prepared by hydrothermal method, *J. Hazard. Mater.*, 2009, **161**, 42–48.

96 S. Yamazoe, T. Okumura, K. Teramura and T. Tanaka, Development of the efficient TiO_2 photocatalyst in photoassisted selective catalytic reduction of NO with NH_3, *Catal. Today*, 2006, **111**, 266–270.

97 S. Yamazoe, Y. Masutani, T. Shishido and T. Tanaka, Metal oxide promoted TiO_2 catalysts for photo-assisted selective catalytic reduction of NO with NH_3, *Res. Chem. Intermed.*, 2008, **34**, 487–494.

98 T. Tanaka, K. Teramura, K. Arakaki and T. Funabiki, Photoassisted NO reduction with NH_3 over TiO_2 photocatalyst, *Chem. Commun.*, 2002, 2742–2743.

99 J. Papp, S. Soled, K. Dwight and A. Wold, Surface Acidity and Photocatalytic Activity of TiO_2, WO_3/TiO_2, and MoO_3/TiO_2 Photocatalysts, *Chem. Mater.*, 1994, **6**, 496–500.

100 S. Yamazoe, Y. Masutani, K. Teramura, Y. Hitomi, T. Shishido and T. Tanaka, Promotion effect of tungsten oxide on photo-assisted selective catalytic reduction of NO with NH_3 over TiO_2, *Appl. Catal., B*, 2008, **83**, 123–130.

101 S. Yamazoe, Y. Masutani, T. Shishido and T. Tanaka, XAFS study of active tungsten species on WO_3/TiO_2 as a catalyst for photo-SCR, *EXAFS Spectrosc.: Tech. Appl., Proc. Symp. Appl. EXAFS Mater. Sci.*, 2007, 696.

102 A. Yamamoto, K. Teramura and T. Tanaka, Selective Catalytic Reduction of NO by NH_3 over Photocatalysts (Photo-SCR): Mechanistic Investigations and Developments, *Chem. Rec.*, 2016, **16**, 2268–2277.

103 Y. Ji, B. Ding, W. Ni, X. Li, X. He, Z. Chen, S. Ran and H. Lü, Tailoring the crystal structure of $CaTiO_3$ by multielement doping for photo-assisted activation of NO, *Chem. Eng. J.*, 2022, **450**, 138255.

104 K. Wei, X. Yan, S. Zuo, W. Zhu, F. Wu, X. Li, C. Yao and X. Liu, Photo-assisted Catalytic Removal of NO_x Over $La_{1-x}Pr_xCoO_3$/Palygorskite Nanocomposites: Role of Pr Doping, *Clays Clay Miner.*, 2019, **67**, 348–356.

105 X. Li, H. Shi, W. Zhu, S. Zuo, X. Lu, S. Luo, Z. Li, C. Yao and Y. Chen, Nanocomposite $LaFe_{1\text{-}x}Ni_xO_3$/Palygorskite catalyst

for photo-assisted reduction of NOx: Effect of Ni doping, *Appl. Catal., B*, 2018, **231**, 92–100.

106 X. Li, H. Shi, X. Yan, S. Zuo, Y. Zhang, T. Wang, S. Luo, C. Yao and C. Ni, Palygorskite Immobilized Direct Z-Scheme Nitrogen-Doped Carbon Quantum dots/$PrFeO_3$ for Photo-SCR Removal of NO_x, *ACS Sustain. Chem. Eng.*, 2018, **6**, 10616–10627.

107 L. Chen, D. Shen, B. Li, Z. Xiao, W. Sun, X. Liu, J. Ma, C. Li and W. Wang, The efficient electrocatalytic and photocatalytic reduction of nitric oxide into ammonia over 0D/3D g-C_3N_4 quantum dots/3DOMM-TiO_{2-x} heterojunction, *Ceram. Int.*, 2023, **49**, 23129–23139.

108 L. Ju, X. Tang, Y. Zhang, X. Li, X. Cui and G. Yang, Single Selenium Atomic Vacancy Enabled Efficient Visible-Light-Response Photocatalytic NO Reduction to NH_3 on Janus WSSe Monolayer, *Molecules*, 2023, **28**(7), 2959.

109 D. Yao, C. Tang, P. Wang, H. Cheng, H. Jin, L.-X. Ding and S.-Z. Qiao, Electrocatalytic green ammonia production beyond ambient aqueous nitrogen reduction, *Chem. Eng. Sci.*, 2022, **257**, 117735.

110 I. G. Zacharia and W. M. Deen, Diffusivity and Solubility of Nitric Oxide in Water and Saline, *Ann. Biomed. Eng.*, 2005, **33**, 214–222.

111 J. Li, J. Wang, S. Shen, R. Chen, M. Liu and F. Dong, Beyond Purification: Highly Efficient and Selective Conversion of NO into Ammonia by Coupling Continuous Absorption and Photoreduction under Ambient Conditions, *Environ. Sci. Technol.*, 2023, **57**, 5445–5452.

112 W. Chen, R. Zou and X. Wang, Toward an Atomic-Level Understanding of the Catalytic Mechanism of Selective Catalytic Reduction of NO_x with NH_3, *ACS Catal.*, 2022, **12**, 14347–14375.

113 Z. Si, Y. Shen, J. He, T. Yan, J. Zhang, J. Deng and D. Zhang, SO_2-Induced Alkali Resistance of $FeVO_4/TiO_2$ Catalysts for NO_x Reduction, *Environ. Sci. Technol.*, 2022, **56**, 605–613.

114 R. Chen, J. Li, J. Wang, W. Yang, S. Shen and F. Dong, Continuous NO Upcycling into Ammonia Promoted by SO_2 in Flue Gas: Poison Can Be a Gift, *Environ. Sci. Technol.*, 2023, **57**, 12127–12134.

115 W. Yang, J. Wang, R. Chen, L. Xiao, S. Shen, J. Li and F. Dong, Reaction mechanism and selectivity regulation of photocatalytic nitrate reduction for wastewater purification: progress and challenges, *J. Mater. Chem. A*, 2022, **10**, 17357–17376.

116 H. Li, H. Zhu, Y. Shi, H. Shang, L. Zhang and J. Wang, Vacancy-Rich and Porous NiFe-Layered Double Hydroxide Ultrathin Nanosheets for Efficient Photocatalytic NO Oxidation and Storage, *Environ. Sci. Technol.*, 2022, **56**, 1771–1779.

117 H. Hirakawa, M. Hashimoto, Y. Shiraishi and T. Hirai, Selective Nitrate-to-Ammonia Transformation on Surface Defects of Titanium Dioxide Photocatalysts, *ACS Catal.*, 2017, **7**, 3713–3720.

118 H. S. Moon, B. Song, J. Jeon, T.-H. Lai, Y.-P. Chang, Y.-D. Lin, J. K. Park, Y.-G. Lin, Y.-J. Hsu, H. Shin, Y. Yun and K. Yong, Atomically isolated copper on titanium dioxide for ammonia photosynthesis via nitrate reduction with unprecedently high apparent quantum yield, *Appl. Catal., B*, 2023, **339**, 123185.

119 J. Li, R. Chen, J. Wang, K. Wang, Y. Zhou, M. Xing and F. Dong, Dynamic in situ Formation of Cu_2O Sub-Nanoclusters through Photoinduced pseudo-Fehling's Reaction for Selective and Efficient Nitrate-to-Ammonia Photosynthesis, *Angew. Chem., Int. Ed.*, 2024, **63**, e202317575.

120 R. Chen, S. Shen, K. Wang, J. Wang, W. Yang, X. Li, J. Li and F. Dong, Promoting the efficiency and selectivity of NO_3^--to-NH_3 reduction on Cu-O-Ti active sites via preferential glycol oxidation with holes, *Proc. Natl. Acad. Sci. U.S.A.*, 2023, **120**, e2312550120.

121 J. Li, R. Chen, J. Wang, Y. Zhou, G. Yang and F. Dong, Subnanometric alkaline-earth oxide clusters for sustainable nitrate to ammonia photosynthesis, *Nat. Commun.*, 2022, **13**, 1098.

122 A. Sanchez, Z. Ye, Y. Yin and H. Liu, Photochemical conversion of nitrate to ammonium ions by a newly developed photo-reductive titanium dioxide catalyst: implications on nitrogen recovery, *Environ. Sci.: Water Res. Technol.*, 2023, **9**, 3318–3324.

123 L. Wei, Y. Zhang, C. Zhang, C. Yao, C. Ni and X. Li, In Situ Growth of Perovskite on 2D Hydrothermal Carbonation Carbon for Photocatalytic Reduction of Nitrate to Ammonia, *ACS Appl. Nano Mater.*, 2023, **6**, 13127–13136.

124 W. Liu, X. Li, X. Chu, S. Zuo, B. Gao, C. Yao, Z. Li and Y. Chen, Boosting photocatalytic reduction of nitrate to ammonia enabled by perovskite/biochar nanocomposites with oxygen defects and O-containing functional groups, *Chemosphere*, 2022, **294**, 133763.

125 Y. Wang, H. Yin, X. Zhao, Y. Qu, A. Zheng, H. Zhou, W. Fang and J. Li, Photocatalytic ammonia synthesis from nitrate reduction on nickel single-atom decorated on defective tungsten oxide, *Appl. Catal., B*, 2024, **341**, 123266.

126 D. Hao, Y. Wei, L. Mao, X. Bai, Y. Liu, B. Xu, W. Wei and B.-J. Ni, Boosted selective catalytic nitrate reduction to ammonia on carbon/bismuth/bismuth oxide photocatalysts, *J. Cleaner Prod.*, 2022, **331**, 129975.

127 R. Kato, M. Furukawa, I. Tateishi, H. Katsumata and S. Kaneco, Novel Photocatalytic NH_3 Synthesis by NO_3^- Reduction over $CuAg/TiO_2$, *Chem. Eng.*, 2019, **3**(2), 49.

128 L. Wei, M. A. S. Adamson and J. Vela, Ni_2P-Modified Ta_3N_5 and TaON for Photocatalytic Nitrate Reduction, *ChemNanoMat*, 2020, **6**, 1179–1185.

129 N. Tong, Y. Wang, Y. Liu, M. Li, Z. Zhang, H. Huang, T. Sun, J. Yang, F. Li and X. Wang, PdSn/NiO/$NaTaO_3$: La for photocatalytic ammonia synthesis by reduction of NO_3^- with formic acid in aqueous solution, *J. Catal.*, 2018, **361**, 303–312.

130 M. Yamauchi, R. Abe, T. Tsukuda, K. Kato and M. Takata, Highly Selective Ammonia Synthesis from Nitrate with Photocatalytically Generated Hydrogen on $CuPd/TiO_2$, *J. Am. Chem. Soc.*, 2011, **133**, 1150–1152.